NASA/TM–2014-218543

Evaluation of the First Transport Rotorcraft Airframe Crash Testbed (TRACT 1) Full-Scale Crash Test

Martin S. Annett, Justin D. Littell, and Karen E. Jackson
Langley Research Center, Hampton, Virginia

Lindley W. Bark
Naval Air System Command, Patuxent River, Maryland

Rick L. DeWeese
Federal Aviation Administration, Oklahoma City, Oklahoma

B. Joseph McEntire
United States Army Aeromedical Research Laboratory, Fort Rucker, Alabama

October 2014

NASA STI Program . . . in Profile

Since its founding, NASA has been dedicated to the advancement of aeronautics and space science. The NASA scientific and technical information (STI) program plays a key part in helping NASA maintain this important role.

The NASA STI program operates under the auspices of the Agency Chief Information Officer. It collects, organizes, provides for archiving, and disseminates NASA's STI. The NASA STI program provides access to the NASA Aeronautics and Space Database and its public interface, the NASA Technical Report Server, thus providing one of the largest collections of aeronautical and space science STI in the world. Results are published in both non-NASA channels and by NASA in the NASA STI Report Series, which includes the following report types:

- TECHNICAL PUBLICATION. Reports of completed research or a major significant phase of research that present the results of NASA Programs and include extensive data or theoretical analysis. Includes compilations of significant scientific and technical data and information deemed to be of continuing reference value. NASA counterpart of peer-reviewed formal professional papers, but having less stringent limitations on manuscript length and extent of graphic presentations.

- TECHNICAL MEMORANDUM. Scientific and technical findings that are preliminary or of specialized interest, e.g., quick release reports, working papers, and bibliographies that contain minimal annotation. Does not contain extensive analysis.

- CONTRACTOR REPORT. Scientific and technical findings by NASA-sponsored contractors and grantees.

- CONFERENCE PUBLICATION. Collected papers from scientific and technical conferences, symposia, seminars, or other meetings sponsored or co-sponsored by NASA.

- SPECIAL PUBLICATION. Scientific, technical, or historical information from NASA programs, projects, and missions, often concerned with subjects having substantial public interest.

- TECHNICAL TRANSLATION. English-language translations of foreign scientific and technical material pertinent to NASA's mission.

Specialized services also include organizing and publishing research results, distributing specialized research announcements and feeds, providing information desk and personal search support, and enabling data exchange services.

For more information about the NASA STI program, see the following:

- Access the NASA STI program home page at *http://www.sti.nasa.gov*

- E-mail your question to help@sti.nasa.gov

- Fax your question to the NASA STI Information Desk at 443-757-5803

- Phone the NASA STI Information Desk at 443-757-5802

- Write to:
  STI Information Desk
  NASA Center for AeroSpace Information
  7115 Standard Drive
  Hanover, MD 21076-1320

NASA/TM–2014-218543

Evaluation of the First Transport Rotorcraft Airframe Crash Testbed (TRACT 1) Full-Scale Crash Test

Martin S. Annett, Justin D. Littell, and Karen E. Jackson
Langley Research Center, Hampton, Virginia

Lindley W. Bark
Naval Air System Command, Patuxent River, Maryland

Rick L. DeWeese
Federal Aviation Administration, Oklahoma City, Oklahoma

B. Joseph McEntire
United States Army Aeromedical Research Laboratory, Fort Rucker, Alabama

National Aeronautics and
Space Administration

Langley Research Center
Hampton, Virginia 23681-2199

October 2014

Available from:

NASA Center for AeroSpace Information
7115 Standard Drive
Hanover, MD 21076-1320
443-757-5802

ABSTRACT

In 2012, the NASA Rotary Wing Crashworthiness Program initiated the Transport Rotorcraft Airframe Crash Testbed (TRACT) research program by obtaining two CH-46E helicopters from the Navy CH-46E Program Office (PMA-226) at the Navy Flight Readiness Center in Cherry Point, North Carolina. Full-scale crash tests were planned to assess dynamic responses of transport-category rotorcraft under combined horizontal and vertical impact loading. The first crash test (TRACT 1) was performed at NASA Langley Research Center's Landing and Impact Research Facility (LandIR), which enables the study of critical interactions between the airframe, seat, and occupant during a controlled crash environment. The CH-46E fuselage is categorized as a medium-lift rotorcraft with fuselage dimensions comparable to a regional jet or business jet. The first TRACT test (TRACT 1) was conducted in August 2013. The primary objectives for TRACT 1 were to: (1) assess improvements to occupant loads and displacement with the use of crashworthy features such as pre-tensioning active restraints and energy absorbing seats, (2) develop novel techniques for photogrammetric data acquisition to measure occupant and airframe kinematics, and (3) provide baseline data for future comparison with a retrofitted airframe configuration. Crash test conditions for TRACT 1 were 33-ft/s forward and 25-ft/s vertical combined velocity onto soft soil, which represent a severe, but potentially survivable impact scenario. The extraordinary value of the TRACT 1 test was reflected by the breadth of meaningful experiments. A total of 8 unique experiments were conducted to evaluate ATD responses, seat and restraint performance, cargo restraint effectiveness, patient litter behavior, and photogrammetric techniques. A combination of Hybrid II, Hybrid III, and ES-2 Anthropomorphic Test Devices (ATDs) were placed in forward and side facing seats and occupant results were compared against injury criteria. Loads from ATDs in energy absorbing seats and restraints were within injury limits. Severe injury was likely for ATDs in forward facing passenger seats, legacy troop bench seats, and a three-tiered patient litter. In addition, two standing ATDs were used to evaluate the benefit of Mobile Aircrew Restraint Systems (MARS) versus a standard gunner's belt. The ATD with the MARS survived the impact, while fatal head blunt trauma occurred for the standing ATD held by the legacy gunner's belt. In addition to occupant loading, the structural response of the airframe was assessed based on accelerometers located throughout the airframe and using three-dimensional photogrammetric techniques. Analysis of the photogrammetric data indicated regions of maximum deflection and permanent deformation.

BACKGROUND

The purpose of NASA's Fundamental Aeronautics Program Rotary Wing Project (FAP RW) is to "develop and validate tools, technologies and concepts to overcome key barriers for rotary wing vehicles." One focal area of FAP RW research is to "foster, develop and demonstrate technologies that are critical to the successful commercial operation and passenger acceptance of large rotary wing transports in NextGen airspace" (ref. 1). Critical to the acceptance and certification of NextGen rotorcraft is the ability to accurately characterize the airframe impact dynamics and imparted occupant loads under crash conditions.

The military crash safety standard for rotorcraft (MIL-STD-1290(A)) specifies occupant seat acceleration limits and occupied volume reduction constraints for seven crash impact design

scenarios. These design scenarios are intended to encompass all weight classes and account for two impact surfaces, rigid and plowed soil (ref. 2). Crashworthy features, such as energy absorbing seats, airbags, and crushable structures, have been designed into rotorcraft such as the AH-64 and UH-60 based on this standard. These design features have resulted in an increase in the 90th percentile survivable longitudinal and vertical impact speeds (ref. 3). A 20-year mishap survey of US Navy aircraft by Kent concluded that non-pilot personnel remain more susceptible to injury and fatality, and current and future crash protection system improvement should address that concern (ref. 4).

A recent DOD study by Couch and Lindell recommended updates to MIL-STD-1290(A) to include a wider range of aircraft classes and impact environments (ref. 5). Recently, the Army Aviation Technology Directorate (AATD) sponsored a cooperative effort resulting in the publication of the Full Spectrum Crashworthiness Criteria (ref. 6). The FSC outlined guidelines for developing comprehensive crash design requirements for a wide range of rotorcraft classes, types, configurations, and operating conditions throughout the life cycle of the rotorcraft. The Crashworthiness Index (CI) has been proposed as new design standard to replace ADS-11B specifications, with a higher score contribution due to basic airframe crashworthiness (ref. 7).

The Federal Airworthiness Standard for transport category rotorcraft (§14 CFR 29.562) does not address crashworthiness at the airframe level (ref. 8). A pair of idealized acceleration vs. time conditions is specified for evaluation of the seat and occupant. Crash sled testing with Anthropomorphic Test Devices (ATDs) must be conducted to determine seat structural adequacy and occupant survivability. Civil seats are often designed with energy absorbers and other collapsible mechanisms to limit the occupant loads. The Federal Aviation Administration (FAA) is currently developing new policy directives that will address applying computational methods in lieu of testing for seat certification (ref. 9). New injury criteria are also being developed by the FAA for both side and oblique facing seats (ref. 10).

The performance of crashworthy systems is optimized primarily for a specific occupant weight (typically 50th percentile males) and assumed idealized input deceleration pulses. However, the response is highly sensitive to any variations from those standards. Multi-terrain impact (water, soft soil, prepared surface) will alter the magnitude and duration of the airframe deceleration. The combination of landing gear stroke, subfloor crushing, floor and frame deformation, seat stroke, and restraint activation must all be taken in account.

Essential in this effort is the development and assessment of modeling tools that can accurately associate impact velocities, attitudes and terrains to seat interface and occupant G-loads. Recent advancements in computational techniques have allowed for streamlined and efficient evaluations of the crash performance of rotorcraft. Finite element models (FEM) have been developed that contain sufficient fidelity to model material damage and failure progression within the airframe during impact and are yet computationally affordable. The analytical capabilities have progressed from vehicle lumped parameter models (KRASH) to multi-body occupant models (MADYMO) to high fidelity explicit finite element analyses (LS-DYNA, PAM-CRASH, Radioss, ABAQUS-Explicit). Detailed representations of seats, occupants, and restraints can be feasibly included in a system-level FEM to accurately account for the load transfer between the airframe and the occupant and to directly assess the likelihood of occupant injury.

The current emphasis in aviation across all categories is incorporation of high performance composite materials into the airframe design to enhance vehicle efficiency. Examples of medium to heavy lift rotorcraft containing more than 20 percent composites by weight include the V-22 Osprey and the CH-53K. The benefit of increased stiffness to weight ratio provided by composites must be balanced against the crashworthiness of the structure. Composite materials have unique considerations for both performance evaluation and certification. The impact dynamics behavior of composites is markedly different than legacy aluminum airframes in terms of failure initiation, damage progression, and specific energy absorption. Analytical tools and material/structural characterization tests are necessary for the design of energy-absorbing composite structures. The current design building block test sequence for material characterization and analysis validation methodologies may not encapsulate all critical modes of failure. Current models are phenomenological and parameters in simulations are determined by calibration from test.

Ultimately, crash safety certification by analysis is sought to minimize reliance on full-scale crash tests. Nonetheless, a requisite number of section-level to full-scale tests must be conducted to anchor simulations of rotorcraft which incorporate novel crashworthy features and composite airframe structures. With the support of the FAP RW Project, two full-scale crash tests were planned to address transport category rotorcraft crash responses under combined horizontal and vertical loading. The Transport Rotorcraft Airframe Crash Testbed (TRACT) full-scale crash tests were proposed. The first test, designated TRACT 1, would evaluate a collection of crashworthy system experiments and characterize the metallic fuselage response to a severe but survivable impact. The second test (TRACT 2) will contain similar experiments but also include a retrofit of the TRACT subfloor with composite energy absorbing concepts. This memorandum is intended to provide specific details regarding TRACT 1.

INTRODUCTION

Test Facility

A photograph of NASA Langley's Landing and Impact Research Facility (LandIR) is shown in Figure 1. The LandIR facility provides the unique capability for full-scale impact testing with combined vertical and longitudinal loading onto prepared surfaces, soil, and water. Combined loading tests are conducted by suspending the test article from the gantry structure using two sets of cables: pullback cables and swing cables. These cables are attached to the airframe at hard points that enable the helicopter to be lifted through its center of gravity. The airframe is lifted using the pullback cables to a specified height and pyrotechnically released following a countdown. Swing cables are configured to form a parallelogram to minimize pitch angular velocity during the pendulum swing prior to impact. For land impact, just prior to ground contact, the supporting cables are pyrotechnically separated. For water impact, the test article is suspended from a carrier platform which remains attached to the swing cables. The test article is pyrotechnically severed from the platform and freely impacts the Hydro-Impact Basin.

The LandIR has 320-channels of data acquisition (DAS) capability to record accelerations, strains, displacements, and forces. Three-dimensional photogrammetry is recorded with as many as 1,000

frames per second and synchronized to DAS results using an IRIG time code generator. External vehicle kinematics and onboard occupant responses are tracked using high speed and high definition ruggedized cameras. Eleven Hybrid II and III ATDs are available ranging in size from 3 year and 6 year old child to 5th to 95th percentile adult.

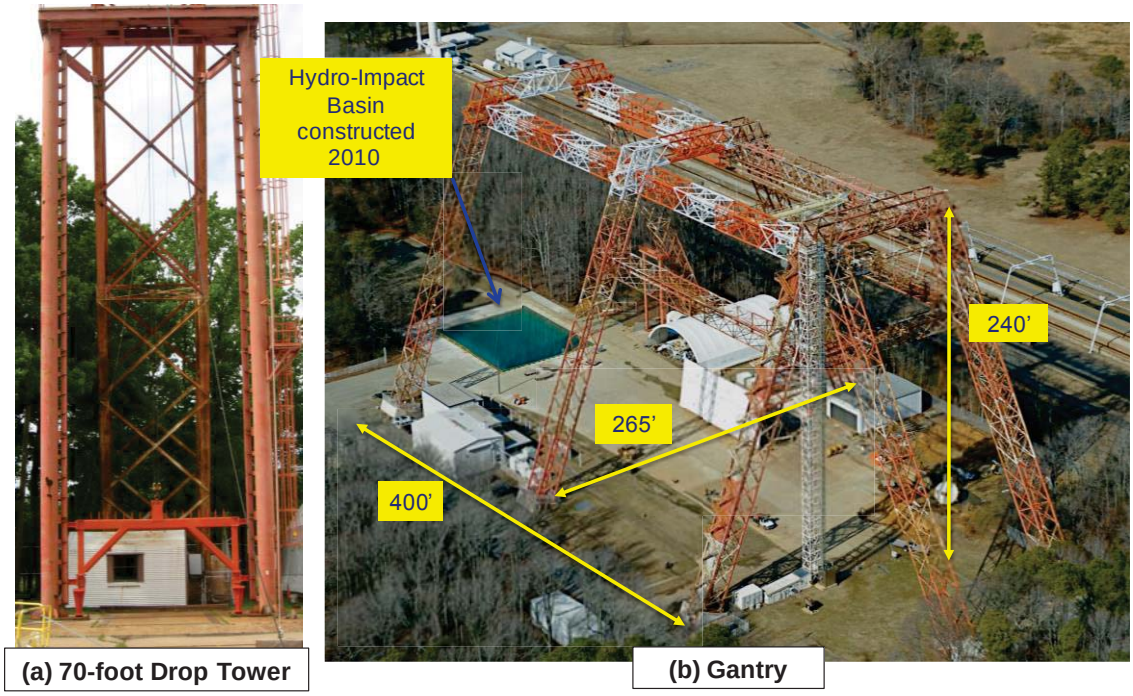

Figure 1. Landing and Impact Research Facility (LandIR)

Test Article

The CH-46E Sea Knight is categorized as a medium-lift tandem rotor helicopter with length and width of nearly 45 ft. and 7 ft., respectively, and a capacity for 5 crew and 25 troops. A schematic drawing is shown in Figure 2 showing Fuselage Station (FS), Water Line (WL), and Butt Line (BL) locations. These dimensions are given in units of inches. The fuselage design is semi-monocoque with skin stiffeners and frame sections. The cabin fuselage cross section is nearly uniform and is composed primarily of Aluminum 2024 and 7075 alloys. Fuselage frames are spaced longitudinally approximately every 30 inches. Between FS120 and FS410, the fuselage section has a nearly uniform cross-section. The FS locations of major structural features are listed in Table 1.

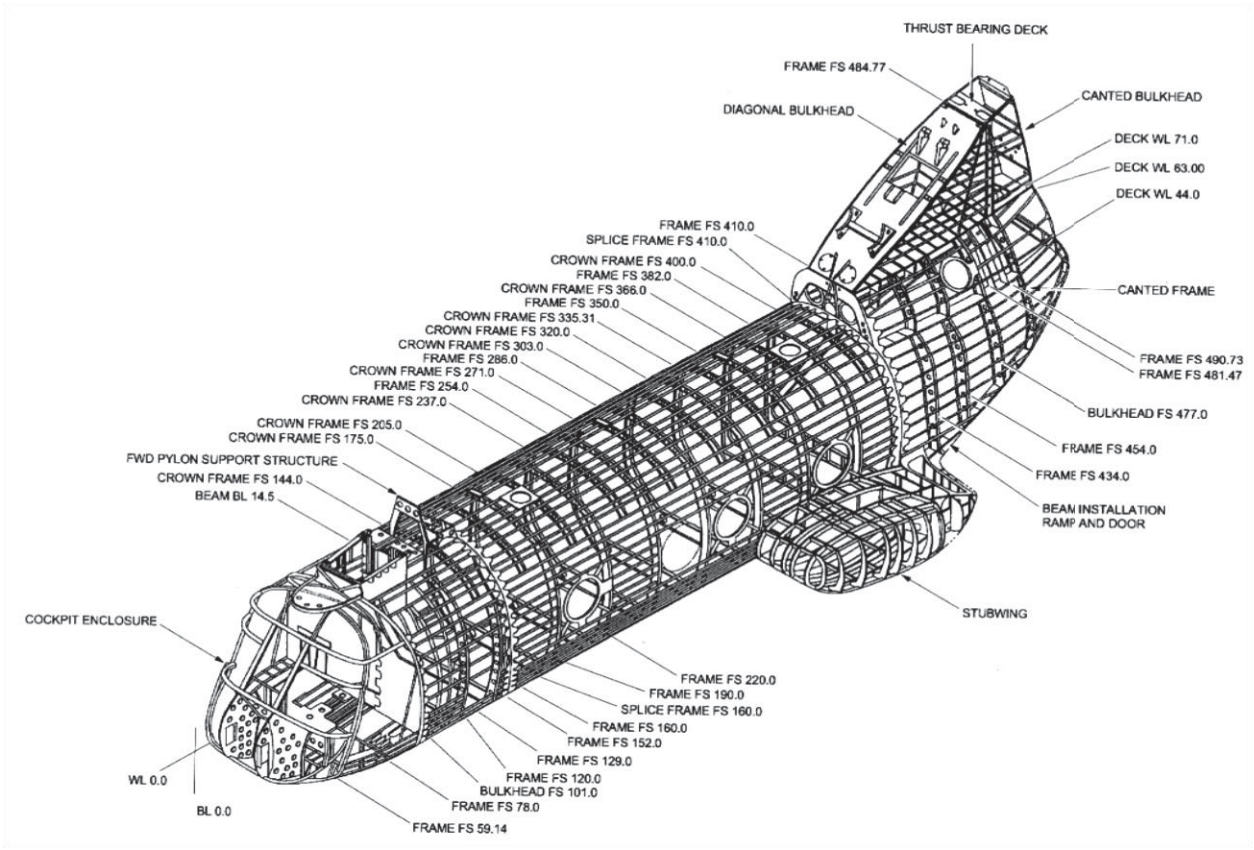

Figure 2. CH-46E airframe schematic with FS, WL, and BL locations highlighted.

Table 1. Longitudinal FS Locations of major structural features

Feature	FS Location
Cockpit and cockpit bulkhead	FS 0 - FS 120
Main cabin	FS 120 – FS 320
Stubwing/aft cabin	FS 320 – FS 410
Tail	FS 410 – FS 490

In 2012, NASA Langley obtained two CH-46E fuselages from the Navy CH-46E Program Office (PMA-226) that were located at the Navy Flight Readiness Center/Cherry Point. The stubwings which hold the main landing gear were removed for testing, along with the vertical tail and engine, rotor, and transmission components. The weight of these components was not replaced, because the fuselage was intended not to mimic the overall weight and center of gravity (CG) of the CH-46E. The main cabin from the cockpit aft bulkhead to the stubwing area contains five frame sections that are nearly identical in spacing and design to allow multiple occupant, seat, and crashworthy systems experiments to be evaluated. The as-delivered bare fuselage weight was approximately 2,500 lb. A photograph of the TRACT 1 airframe is shown in Figure 3.

.

Figure 3. TRACT 1 fuselage

Modifications were made to the TRACT structure before installation of the experiments. The aluminum honeycomb floor was reinforced underneath to provide hard points for mounting seats and other experiments. Two swing beams were bolted to the sidewalls approximately 3 inches above the waterline to provide a sturdy interface for the swing and pullback cables. Fiberglass panels were fabricated and attached to the underside of the cockpit enclosure to reduce plowing of the exposed cockpit.

Collaborators

The primary objective for TRACT 1 was to evaluate the integrated airframe, seat, and occupant responses under a combined horizontal and vertical impact velocity. This test article provided an exceptional opportunity for numerous onboard experiments, seat configurations, and ATDs to be included and evaluated. Discussions with crashworthiness and injury biomechanics organizations within the Federal Aviation Administration (FAA), Department of Defense (DOD), and rotorcraft industry manufacturers led to formal agreements with four collaborators:

- The Naval Air Systems Command (NAVAIR), Human Systems Department, Crashworthy Systems Branch, Patuxent River, MD, develops, evaluates, and qualifies systems for Naval Aviation intended to prevent injury resulting from impact-based aviation mishaps.
- The FAA Civil Aeromedical Institute (CAMI), Aeromedical Research Division, Protection and Survival Laboratory, Biodynamics Research Team, conducts research concerning occupant impact protection in civil aircraft. To evaluate the protection provided by seats and restraint systems, the team develops new testing protocols, test dummy modifications and new injury criteria.
- The U.S. Army Aeromedical Research Laboratory (USAARL), Warfighter Protection Division, Injury Biomechanics Branch, investigates air and ground warfighter response to dynamic loading, including blast, ballistics, and impact.
- Cobham Life Support develops restraint systems for fixed and rotary wing and ground vehicles.

Experiments

Test Objective 1: Comparison of the CH-46 crew seat with MA-16 inertia reel and CH-46 crew seat with PARS.

The CH-46E crew seat contains two pairs of energy absorbers (EAs). One pair of variable-load EAs, aligned aft of the seat back, is designed to stroke and limit the loads along the spinal direction. A second pair of fore/aft-oriented EAs limits the seat rail interface loads and prevents detachment of the seat during forward deceleration and occupant flail. The pilot seat is shown in Figure 4.

Figure 4. CH-46E crew seat

Five-point restraints are used with the CH-46E seat. The shoulder webbings are spooled onto the MA-16 inertia reel, which locks passively under inertial loads. As much as 5 inches of extra webbing payout is possible due to pack-down on the spool and elongation due to flail, or forward body displacement. The Pre-Tensioning Aircrew Restraint System (PARS) system is intended to decrease the payout through pyrotechnically actuated spool retraction. Cobham Life Support provided the MA-16 reels, and the PARS pretensioning devices and control modules. The PARS system can be activated with customary crash sensors. For the TRACT 1 test, the PARS was activated at the point of impact with redundant contact switches mounted on the aft belly region. The MA-16 inertia reel and PARS system are located behind the seat back in between the vertical EAs, as shown in Figure 5.

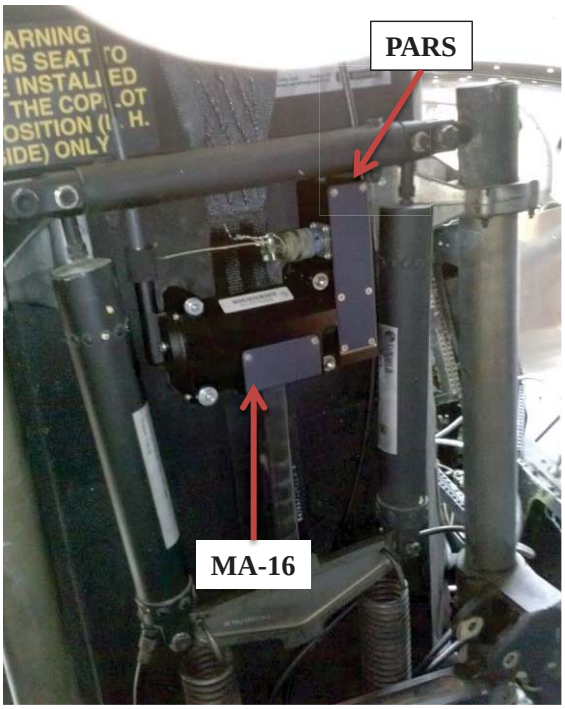

Figure 5. MA-16 inertia reel with PARS

NAVAIR provided two fully instrumented 50th percentile Aerospace Hybrid III ATDs for the pilot and co-pilot seats. The ATDs were outfitted with standard flight suits, helmets, and flight gear. The test article did not have a cockpit enclosure forward of the directional pedals. Therefore, aluminum floor pans were added underneath the feet to ensure loads could be distributed through both the legs and the pelvis. The cockpit ATDs are shown in Figure 6.

Figure 6. Cockpit ATDs

Test Objective 2: Floor-mounted passenger ATD response

The civilian standard for transport category rotorcraft (14 CFR 29.562) specifies two distinct impact conditions that must be tested or analyzed to determine seat adequacy and occupant protection (ref. 8). Tests are normally conducted using acceleration or deceleration crash sleds and a seated 50th percentile Hybrid II or 50th percentile FAA Hybrid III ATD. The first test combines vertical and longitudinal deceleration with a seat pitched 60 degrees relative to the sled velocity vector. The impact velocity is 30 feet per second with a rise time of no more than 0.031 seconds, resulting in a peak deceleration of 30 g. The second test is mostly longitudinal, with no seat pitch and a yaw angle of 10 degrees. The impact velocity is 42 feet per second, with a rise time of no more than 0.071 seconds, resulting in a peak deceleration of 18.4 g. Seat compliance is based on evaluation of whether the seat detaches from the rails, the seat frame collapses, or the seat rails excessively warp. Occupant compliance involves two criteria. If head blunt trauma occurs, the Head Injury Criteria (HIC) index, which is computed through integration of the resultant head acceleration time history, cannot exceed a value of 1,000. Lumbar compressive loads, measured from a load cell below the straight lumbar spine block, cannot be greater than 1,500 lb. For lap belt only configurations, no restraint limits are specified. For a three-point shoulder belt, shoulder restraint loads cannot exceed 1,750 lb. For a four or five point harness, shoulder restraint loads cannot exceed 2,000 lb. For both tests, the input acceleration pulse shapes are triangular.

There are two predominant mechanisms of energy absorption that occur within the cabin during impact, seat frame and cushion distortion, and floor and subfloor web deformation. The timing and interaction of these mechanisms, combined with the occupant flail response, influence the resultant occupant dynamic loading. It is valuable to compare the response of the seat interface in a full-scale crash test environment against the idealized input pulses prescribed for certification.

Two pairs of passenger aircraft seating systems certified to Part 25 standards (ref. 11) were donated by aircraft seat manufacturers. The first seat pair contained a diagonal strut to absorb loads. The second seat pair contained lightweight seat legs without dedicated energy absorbers. Seat legs were adjusted and centered to 23 inches of spacing to share a single pair of seat rails. Four LandIR ATDs were used for these seats. A 50th percentile Hybrid II and 50th percentile FAA Hybrid III were seated in the first pair. A 5th percentile female and a 95th percentile male were seated in the second pair. The floor mounted cabin seats with ATDs are shown in Figure 7. The floor at FS 254 was also loaded with 400 lb. of ballast mass to provide mass loading on the subfloor comparable to two pairs of seats.

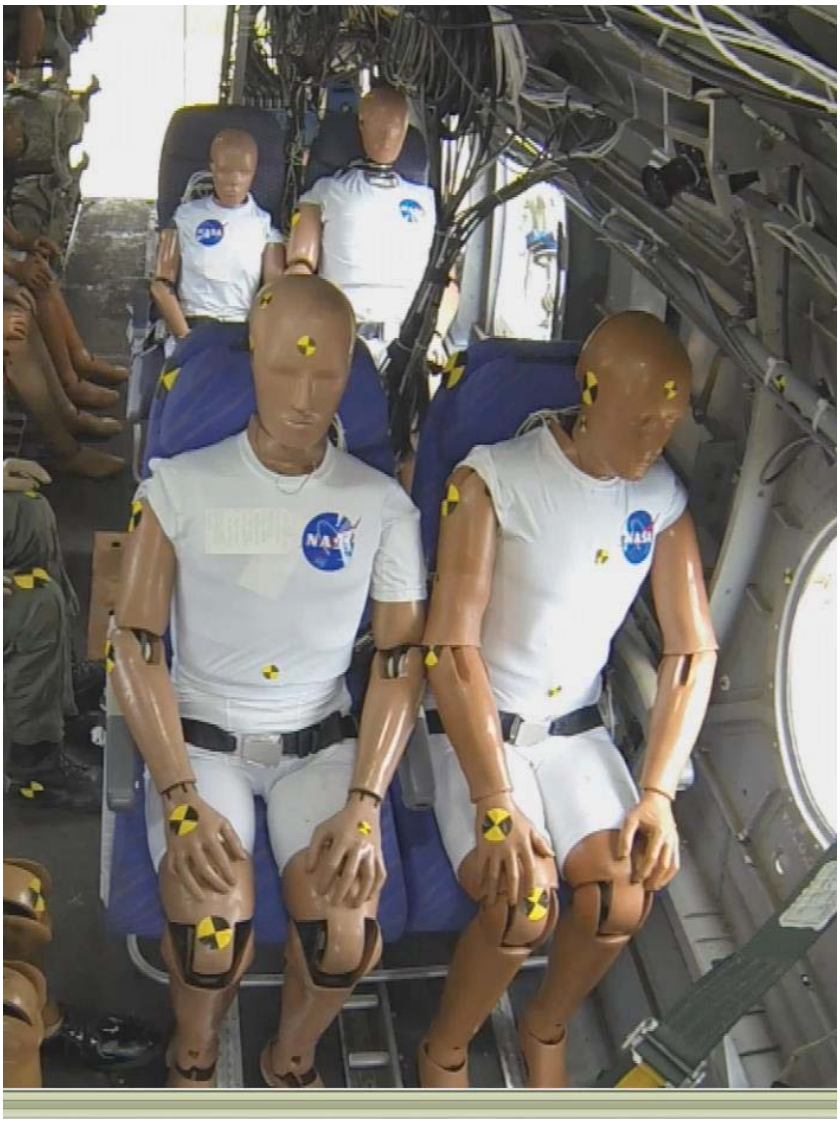

Figure 7. Floor-mounted cabin seats with ATDs

Test Objective 3: Comparison of standing ATD with traditional gunner's belt and standing ATD with Aircrew Endurance Vest and Mobile Aircrew Restraint System (MARS).

Aircrews working within military helicopters are regularly tethered to various anchor points in the cabin to protect against falls during a mishap. This tether is a nylon strap commonly known as a gunner's belt. The gunner's belt is tied to a chest strap and is typically adjusted to the longest length possible for ease of mobility. Mishap data suggests that a slackened gunner's belt may cause injury and fatality during mishaps from strap entanglement, crew impact with structure, or crew excursion. A gunner's belt system that can extend and retract as the crew moves about the cabin is preferable to reduce the strike envelope.

The MARS system was developed by Cobham Life Support as a variation on the MA-16 inertia reel (ref. 12). The MARS mounted in the TRACT test article is shown in Figure 8. The reel can be mounted along multiple cabin ceiling locations, and extends and retracts the webbing as the aircrew moves about the cabin. In a mishap, the retractor locks and slack is minimized. The MARS has been evaluated at the component and crash sled level under dynamic loads, and in flight tests, but not in a full-scale combined velocity impact environment.

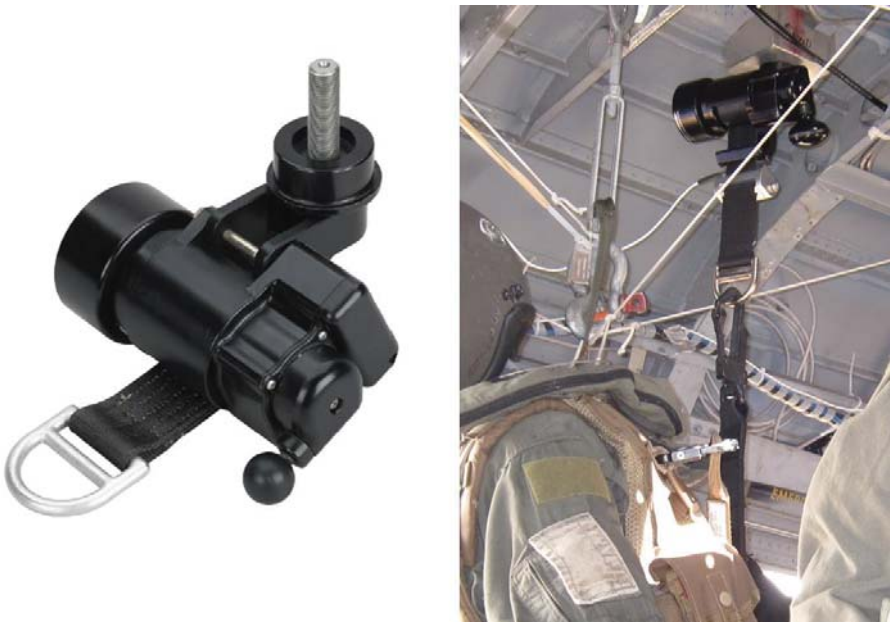

Figure 8. MARS

NAVAIR provided (2) fully instrumented 5th percentile male Aerospace Hybrid III ATDs, one attached to the MARS, and one attached to a standard gunner's belt. The smaller 5th percentile ATDs were used due to cabin height. To secure the standing ATDs in position during pullback and swing, the back of each neck was supported by thin steel cabling, and stabilized by parachute cords. A single pyrotechnic cable cutter was used to sever the steel cable at the point of impact. Hook and loop pads were used to hold boots in place. A photograph showing both standing ATDs is shown in Figure 9.

Figure 9. Standing ATDs

Test Objective 4: Full-field photogrammetry experiment.

Full-field deformation techniques, which include scanning vibrometers, various types of interferometry techniques and digital image correlation, have become more commonplace within the past decade. Digital image correlation applications have vastly expanded due to the advancements of computer processing power required for pattern recognition algorithms, increasing robustness of the sensor hardware, and cost reductions. Novel application ideas have allowed these techniques to shift from strain gauge systems in laboratory data acquisition devices to established data acquisition techniques in the field.

Onboard data recorders provide some indication of impact parameters such as speed and angle during a mishap. Typically, forensic reconstruction techniques can also piece together what happened; however, the actual loads and precise deformation on the airframe are usually unknown. One advantage of controlled crash testing is the capability to measure the damage progression of the airframe. The full-field deformation imaging technique was used in this instance to determine, for the first time, quantitatively, the overall deformation characteristics of a large vehicle airframe during a realistic impact event.

Two monochrome high speed cameras viewed and recorded images of the impact from slightly different angles at a rate of 500 frames per second resulting in pairs of synchronized images of the

impact. A random pattern of over 8,000 1-inch diameter dots was applied to the port airframe skin from the cockpit to the tail. After a camera calibration procedure is completed, the cameras are able to determine the position of each airframe dot in space. Pattern recognition algorithms sense relative deformation between dot groups and an entire deformation field is constructed. The dot pattern for the TRACT and an example of a fringe plot overlay is shown in Figure 10. During test preparation, the airframe was loaded onto a trailer and pulled across the gantry to calibrate the photogrammetry system. The colors in Figure 10 represent relative distance traveled based on a fixed camera location.

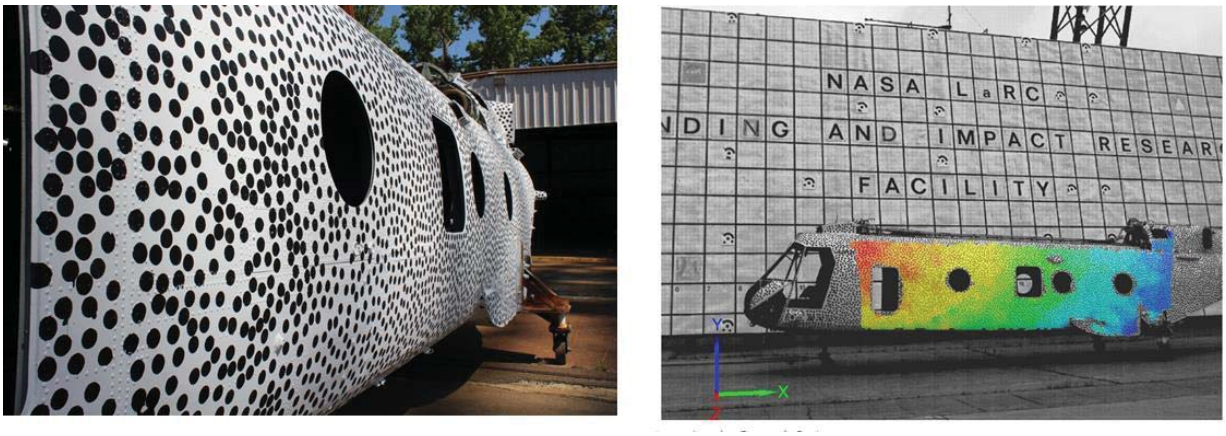

Figure 10. Full-field photogrammetry, strain pattern

Test Objective 5: Comparisons of sidewall-mounted Crew Attenuating Crew Seat (CACS) troop seated Hybrid III ATD, seated Hybrid III ATD with ES-2re head and neck, and two seated Hybrid II ATDs in a standard CH-46 tube and rag sidewall troop seat.

The FAA dynamic test requirements described for Experiment 2 were specifically intended to address forward and aft facing seats. FAA research has shown that passengers in side-facing seats are exposed to injury risks from head and upper extremity flail and pelvic excursion that are not observed for passengers in forward or aft-facing seats (ref. 10). To address the safety of side-facing seats in transport category aircraft, the FAA provided policy guidance that adopted portions of the automotive side-facing requirements, including use of the ES-2re ATD. The ES-2re is designed to evaluate the injury potential of contact and inertial loads produced during a side impact. Since the automotive side-facing standards do not address neck loading, it was necessary for the FAA to sponsor development of new upper neck injury criteria. Much of the FAA side facing seat research was conducted on crash sleds that introduce lateral loads. The TRACT test provides the opportunity to include both lateral and vertical loading in a realistic impact scenario.

The CH-46E troop seats are side-facing. The legacy CH-46E troop bench is an aluminum seat pan frame with canvas mesh overwrap and lap restraints. The CH-46E Crew Attenuating Crew seat (CACS) is an energy absorbing foldable seat with a five-point restraint. Two wire bender struts provide vertical load limiting capability for the restrained occupant. The typical troop bench and CACS configurations are illustrated in Figure 11.

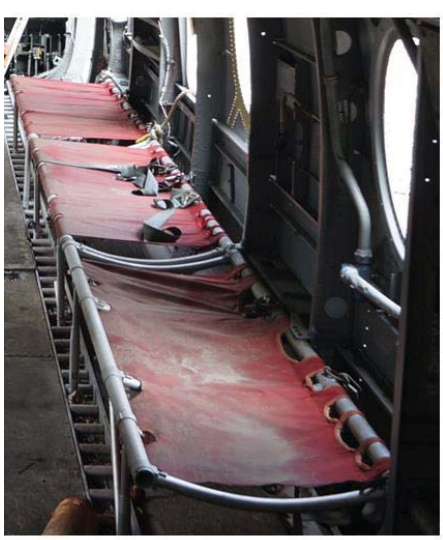

Troop Bench

CACS Seat in Crew Chief and troop position

Figure 11. CH-46E troop seats

CAMI provided a fully instrumented FAA 50th percentile Hybrid III ATD with an ES-2re head and neck for use on one CACS seat. The FAA Hybrid III construction differs from the standard model by including components to permit accurate evaluation of injury risks due to vertical (through the spine) loads. The ES-2re head and neck components provide more biofidelic head/neck kinematics in the lateral direction and injury criteria are available to relate the neck loads measured to injury risk. NAVAIR provided a fully instrumented 50th Aerospace Hybrid III ATD in a second CACS seat for comparison to the CAMI ATD. The Aerospace Hybrid III can also evaluate injury risk from vertical loading. It uses a "pedestrian" pelvis assembly that provides more freedom of motion for the lower legs than provided by the "sitting" pelvis design of the FAA Hybrid III. Both Hybrid III models have shoulder and hip construction that provide consistent belt interaction. Figure 12 shows the CACS side-facing ATDs. Two 50th percentile Hybrid II LandIR ATDs were seated on the troop bench and restrained with lap belts (Figure 13). It was anticipated the troop bench would not survive the impact undamaged. Therefore, the troop bench experiment functioned mostly as a performance benchmark when evaluating the response of side-facing occupants.

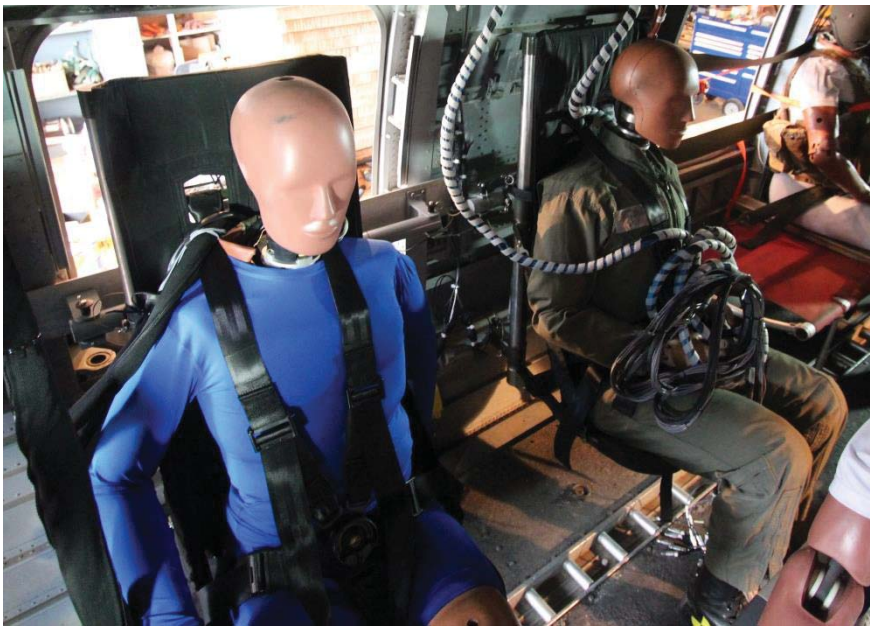

Figure 12. CACS side-facing ATDs

Figure 13. Troop bench ATDs

Test Objective 6: Evaluation of markerless tracking on ATD response.

Traditional tracking systems use targets, stickers, paint or other externally applied features which discriminate specific areas (or targets) on the object. Target motion is captured with high speed cameras to measure kinematic motion and flail envelope. The development in markerless tracking capabilities and systems could potentially change the way measurements are made on ATDs. Markerless tracking systems use their own projection/acquisition system to acquire data on either specific features or on the entire object without the aid of external markers. These measurement systems are still in development, but some of the early systems show promise as an alternative or supplement to either the conventional tracking systems or the internal sensor suite.

An experiment to utilize commercial markerless tracking hardware within a dynamic impact environment was proposed. The standing ATD with the MARS restraint provided a suitable target for tracking. The commercial hardware consisted of a color digital video camera, along with a depth sensor/camera and an infrared projector combined in one package. The depth sensor and infrared projector worked in conjunction to obtain depth measurements in the field of view via a projection/comparison system. The infrared projector projected an infrared dot grid into the field of view, while the depth sensor measured the distance between all of the individual projected dots. The sensor then compared the calculated distances to a calibrated value. The difference between these two values was the measured depth of the projected dots under interrogation. When measured over the entire field of view, a full field depth field was generated. Internal logic preprogrammed with the sensor further examined the depth field and determined the presence of a human by employing various edge detection and area centroid algorithms. If a human shape was detected, a "best fit" three-dimensional skeletal wireframe could then be computed. The wireframe data can be manipulated to give three-dimensional positional time histories of 19 individual joint locations present in the body. From time histories of the joint locations, joint forces could be related to conventional ATD injury criteria. Figure 14 shows the camera field of view and depth fringe plot.

Figure 14. Markerless Tracking

Test Objective 7: Comparison of cargo experiment with non-energy-absorbing restrained cargo mass and energy absorbing restraint cargo mass.

Military and civilian crashworthiness standards require retention of high mass items such as equipment, luggage, or cargo during a mishap. High mass cargo is often restrained to cargo holds and side walls with netting or straps. As the cargo reacts against the restraints, the loads transmitted at the restraint supports can exceed the structural capability of the interface, and the restraints can break free. An optimal cargo restraint design is robust enough to withstand the deceleration of the cargo without structural failure at the interface.

A load-limiting cargo restraint was developed by Penn State University that uses a stitch ripping device (SRD). Energy is absorbed by webbing extension, thread rupture and stitch slippage. The restraint was attached to a breakaway fitting rated for 5,000 lb. failure load. The fitting was then connected to a 500 lb. sliding mass. A standard nylon webbing restraint was also evaluated alongside the SRD restraint with the same breakaway fitting and sliding mass. With 10 g deceleration, the loads would be exceeded in the standard restraint, causing detachment of the mass. The load-limiting restraint was designed to limit to 3,000 lb., and would therefore stroke without fitting detachment. The load-limiting experiment is shown in Figure 15. It was fabricated to be self-contained on a platform that could be bolted to the aft TRACT cabin floor. Housings were assembled around the masses for containment during deceleration.

Figure 15. Cargo Restraint Experiment

Test Objective 8: Three-tiered litter mounted in the aft starboard region of the aircraft cabin.

Legacy litter systems in military rotorcraft have been qualified under static loading. These standards have not been updated in the same manner as have crashworthy seats. An understanding of the performance of the litters and supine litter patients in a crash-induced dynamic loading event is not well understood.

The litter experiment involved a combination of DOD resources. USAARL supplied a three-tiered litter stanchion system compatible with the CH-46. The stanchion interfaces with existing sidewall, ceiling, and cargo rail supports. Two litters, one instrumented 50th Aerospace Hybrid III ATD, and one 200 lb. Grumman-Alderson Research Dummy (GARD) manikin were provided by the USAARL. NAVAIR provided one litter and a second GARD manikin. The two GARD manikins provided the proper mass loading of the litter, which is depicted in Figure 16.

Figure 16. Patient litter experiment

Instrumentation Plan

For TRACT 1, 353-channels of data were collected at 10,000 samples per second using onboard digital data acquisition systems. Schematics of the experiments, instrumentation layout, and cameras are provided in Figures 17-23. In addition, the channel number and sensor types for each airframe location or experiment are listed in Table 2. Tables 3-6 list the individual ATD instrumentation channels. The overall distribution of instrumentation is:

- 279 channels devoted to internal instrumentation of the ATDs and restraint load cells

- 61 channels designated for accelerometers that were mounted on blocks at stiff interfaces between frames and skin, or on ballast weight
- 6 channels for lifting cable load cells
- 7 IRIG time code channels for synchronization with high speed cameras

CAMI provided a DAS rack that linked with the LandIR DAS system and would record all responses for their ATD. USAARL provided DAS racks that were also linked with the LandIR DAS system and would record litter instrumentation along with other sensors located in the aft cabin. The LandIR, CAMI, and USAARL DAS racks were connected in series to receive common trigger, onboard battery power, and DAS software control. NAVAIR supplied a separate DAS that was compatible with the NAVAIR ATD instrumentation. The NAVAIR DAS was independently controlled and powered with onboard batteries. The DAS racks were installed at two locations on the cockpit bulkhead and on a sidewall-mounted shelf aft of the second forward facing seat pair.

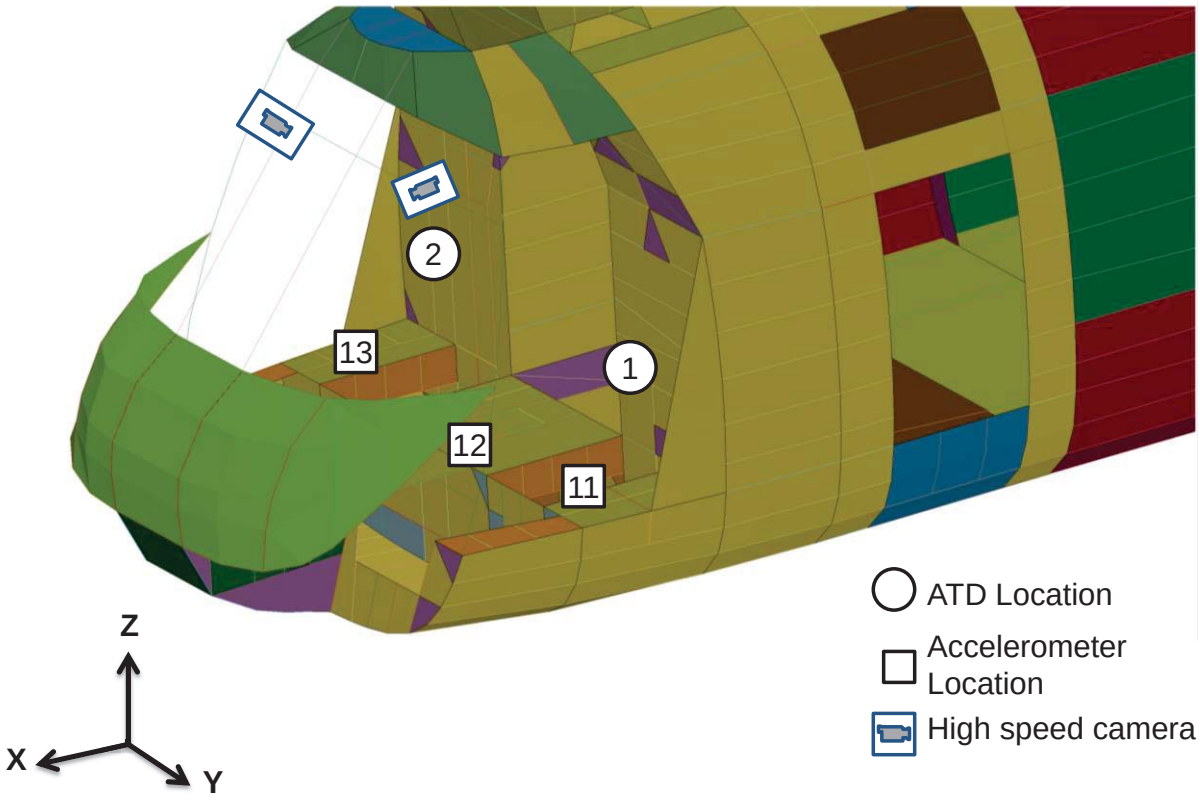

Figure 17. Cockpit instrumentation

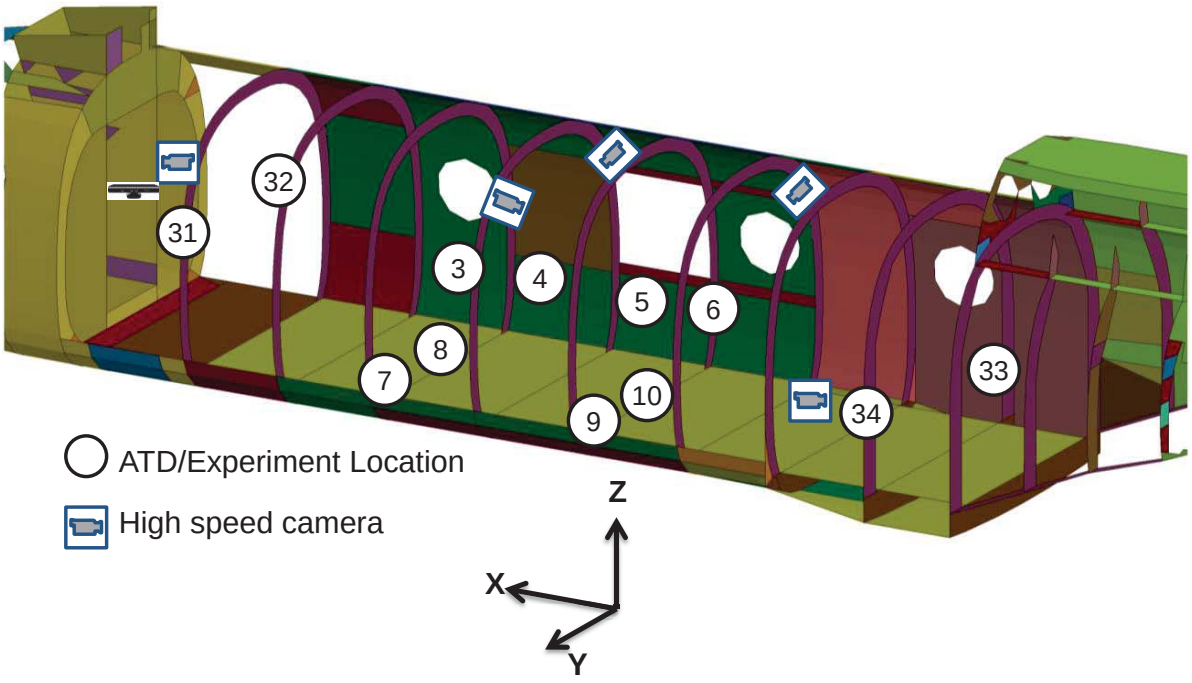

Figure 18. Cabin instrumentation- ATD and high speed camera, isometric view

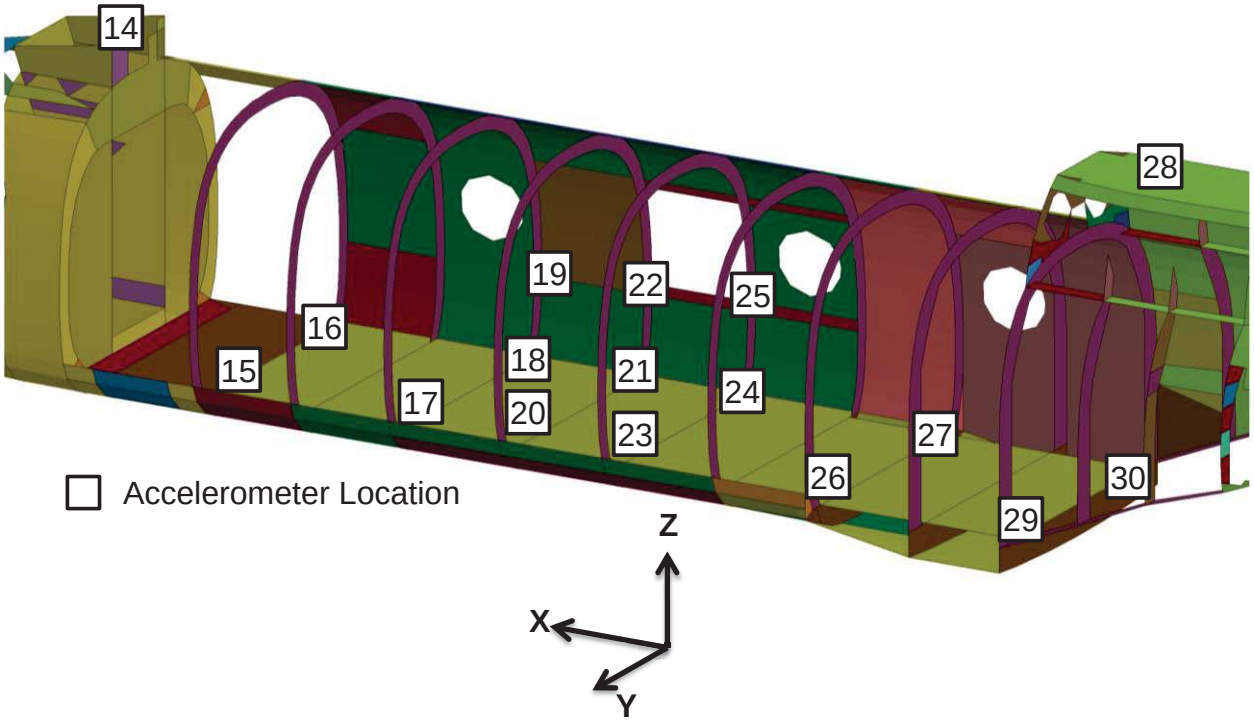

Figure 19. Cabin instrumentation- accelerometers

Table 2. Data acquisition instrumentation list

Position	Measurement	Location	Notes	Total # of Channels
1	ATD Aerospace Hybrid III 50th male (*NAVAIR*)	Co-pilot (front left)	Accelerometers, spinal load cells, shoulder strap load cells	28
2	ATD Aerospace Hybrid III 50th male (*NAVAIR*)	Pilot (front right)	Accelerometers, spinal load cells, shoulder strap load cells	28
3	ATD Hybrid III/ES-2 Neck (*CAMI*)	Cabin (side-facing CACS Seat)	Accelerometers, spinal load cells, shoulder strap load cells	51
4	ATD Aerospace Hybrid III 50th male (*NAVAIR*)	Cabin (side-facing CACS Seat)	Accelerometers, spinal load cells, shoulder strap load cells	28
5	ATD Hybrid II 50th male (*NASA LandIR*)	Cabin (side-facing troop bench)	Accelerometers, spinal load cells, lap strap load cells	11
6	ATD Hybrid II 50th male (*NASA LandIR*)	Cabin (side-facing troop bench)	Accelerometers, spinal load cells, lap strap load cells	11
7	ATD Hybrid II 50th male (*NASA LandIR*)	Cabin (forward facing passenger seat)	Accelerometers, spinal load cells, lap strap load cells	11
8	ATD FAA Hybrid III 50th male (*NASA LandIR*)	Cabin (forward facing passenger seat)	Accelerometers, spinal load cells, lap strap load cells	17
9	ATD Hybrid III 95th male (*NASA LandIR*)	Cabin (forward facing passenger seat)	Accelerometers, spinal load cells, lap strap load cells	17
10	ATD Hybrid III 5th female (*NASA LandIR*)	Cabin (forward facing passenger seat)	Accelerometers, spinal load cells, lap strap load cells	17
11	Acceleration	Co-pilot (front left floor)	X, Z	2
12	Acceleration	Between pilot-co-pilot	X, Y, Z	3
13	Acceleration	Pilot (front right floor)	X, Z	2
14	Acceleration	Main Rotor	X, Y, Z	3
15	Acceleration	Cockpit/cabin fuselage splice, left floor (FS 160.0)	X, Y, Z	3
16	Acceleration	Cockpit/cabin fuselage splice, right floor (FS 160.0)	X, Y, Z	3
17	Acceleration	Cabin Fuselage, left floor (FS 220.0)	X, Z	2
18	Acceleration	Cabin Fuselage, right floor (FS 220.0)	X, Z	2
19	Acceleration	Cabin Fuselage, right side wall (FS 220.0)	X, Z	2
20	Acceleration	Cabin Fuselage, left floor (FS 254.0)	X, Z	2
21	Acceleration	Cabin Fuselage, right floor (FS 254.0)	X, Z	2

Position	Measurement	Location	Notes	Total # of Channels
22	Acceleration	Cabin Fuselage, right side wall (FS 254.0)	X, Z	2
23	Acceleration	Cabin Fuselage, left floor (FS 286.0)	X, Z	2
24	Acceleration	Cabin Fuselage, right floor (FS 286.0)	X, Z	2
25	Acceleration	Cabin Fuselage, right side wall (FS 286.0)	X, Z	2
26	Acceleration	Cabin Fuselage, left floor (FS 350.0)	X, Y, Z	3
27	Acceleration	Cabin Fuselage, right floor (FS 350.0)	X, Y, Z	3
28	Acceleration	Aft Rotor	X, Y, Z	3
29	Acceleration	Cabin Fuselage, left floor (FS 410.0)	X, Z	2
30	Acceleration	Cabin Fuselage, right floor (FS 410.0)	X, Z	2
31	Pedestrian ATD (5th HIII)	Aft of forward bulkhead	Accels, Gunner's belt webbing	10
32	Pedestrian ATD (5th HIII)	Aft of forward bulkhead	Accels, MARS webbing	10
33	Litter ATD	Aft Cabin (near FS 382.0)	Litter interfaces forces and accels	51
34	Cargo restraint	Aft Cabin (near FS 382.0)	Accels and load cells on masses	11
NA	Load cell	4 Swing, 2 Pullback cables	10,000-lb capacity	6

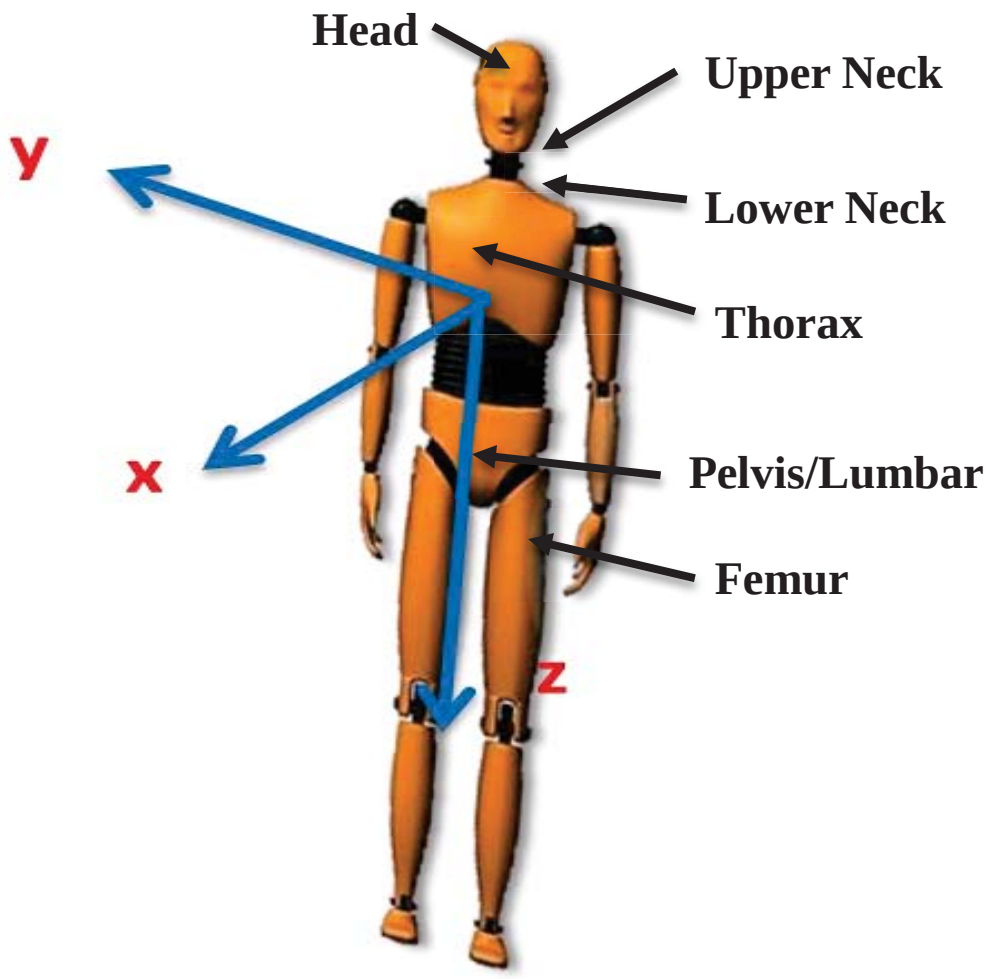

Figure 20. ATD Coordinate System and instrumentation Location

Table 3. NAVAIR ATDs

NAVAIR Hybrid III Channel Count	NAVAIR Pedestrian 5th Channel Count
1 Head A_x	1 Head A_x
2 Head A_y	2 Head A_y
3 Head A_z	3 Head A_z
4 Upper Neck Fx	4 Upper Neck Fz
5 Upper Neck Fy	5 Upper Neck Mx
6 Upper Neck Fz	6 Upper Neck My
7 Upper Neck Mx	7 Chest A_x
8 Upper Neck My	8 Chest A_y
9 Upper Neck Mz	9 Chest A_z
10 Lower Neck Fx	10 Chest Deflection
11 Lower Neck Fy	
12 Lower Neck Fz	
13 Lower Neck Mx	
14 Lower Neck My	
15 Lower Neck Mz	
16 Chest A_x	
17 Chest A_y	
18 Chest A_z	
19 Pelvic A_x	
20 Pelvic A_y	
21 Pelvic A_z	
22 Lumbar Fx	
23 Lumbar Fx	
24 Lumbar Fz	
25 Lumbar Mx	
26 Lumbar My	
27 Lumbar Mz	
28 Strap Load (on shoulder belt)	

Table 4. FAA Hybrid III/ES-2 50th ATD channel count

1 HIII Head Ax
2 HIII Head Ay
3 HIII Head Az
4 HIII Head Rx ARS18K
5 HIII Head Ry ARS18K
6 HIII Head Rz ARS18K
7 ES2 Upper Neck Fx
8 ES2 Upper Neck Fy
9 ES2 Upper Neck Fz
10 ES2 Upper Neck Mx
11 ES2 Upper Neck My
12 ES2 Upper Neck Mz
13 HIII Lower Neck Fx
14 HIII Lower Neck Fy
15 HIII Lower Neck Fz
16 HIII Lower Neck Mx
17 HIII Lower Neck My
18 HIII Lower Neck Mz
19 HIII Thorax Ax
20 HIII Thorax Ay
21 HIII Thorax Az
22 HIII Thorax Rx ARS12K
23 HIII Thorax Ry ARS12K
24 HIII Thorax Rz ARS12K
25 Thoracic Fx
26 Thoracic Fy
27 Thoracic Fz
28 Thoracic Mx
29 Thoracic My
30 HIII Pelvis Ax
31 HIII Pelvis Ay
32 HIII Pelvis Az
33 HIII Pelvis Rx ARS12K
34 HIII Pelvis Ry ARS12K
35 HIII Pelvis Rz ARS12K
36 HIII Lumbar Fx
37 HIII Lumbar Fy
38 HIII Lumbar Fz
39 HIII Lumbar Mx
40 HIII Lumbar My
41 HIII Lumbar Mz
42 Left Femur Rx ARS18K
43 Left Femur Ry ARS18K
44 Left Femur Rz ARS18K
45 Right Femur Rx ARS18K
46 Right Femur Ry ARS18K
47 Right Femur Rz ARS18K
48 Upper Left Shoulder Strap
49 Upper Right Shoulder Strap
50 Left Lap Belt
51 Right Lap Belt

Table 5. USAARL ATD channel count

1 Head AX	31 Right Femur MX
2 Head AY	32 Right Femur MY
3 Head AZ	33 Right Femur MZ
4 Neck FX	34 Fwd Litter Strap z
5 Neck FY	35 Fwd Litter Strap y
6 Neck FZ	36 Fwd Litter Strap x
7 Neck MX	37 Aft Litter Strap z
8 Neck MY	38 Aft Litter Strap y
9 Neck MZ	39 Aft Litter Strap x
10 Chest AX	40 Fwd Wall Mount z
11 Chest AY	41 Fwd Wall Mount y
12 Chest AZ	42 Fwd Wall Mount x
13 Lumbar Spine FX	43 Aft Wall Mount z
14 Lumbar Spine FY	44 Aft Wall Mount y
15 Lumbar Spine FZ	45 Aft Wall Mount x
16 Lumbar Spine MX	46 Top Fwd Belt
17 Lumbar Spine MY	47 Top Litter Aft Belt
18 Lumbar Spine MZ	48 Mid Fwd Belt
19 Pelvis AX	49 Mid Aft Belt
20 Pelvis AY	50 Btm Litter Fwd
21 Pelvis AZ	51 Btm Litter Aft Belt
22 Left Femur FX	
23 Left Femur FY	
24 Left Femur FZ	
25 Left Femur MX	
26 Left Femur MY	
27 Left Femur MZ	
28 Right Femur FX	
29 Right Femur FY	
30 Right Femur FZ	

Table 6. NASA LandIR ATDs

NASA Hybrid III Channel Count (5th,50th,95th)	NASA Hybrid II Channel Count
1 Head A_x	1 Head A_x
2 Head A_y	2 Head A_y
3 Head A_z	3 Head A_z
4 Upper Neck Fx	4 Chest A_x
5 Upper Neck Fz	5 Chest A_y
6 Upper Neck My	6 Chest A_z
7 Lower Neck Fx	7 Lumbar Fz
8 Lower Neck Fz	8 Pelvic A_x
9 Lower Neck My	9 Pelvic A_y
10 Chest A_x	10 Pelvic A_z
11 Chest A_y	11 Strap Load (on lap belt)
12 Chest A_z	
13 Lumbar Fz	
14 Pelvic A_x	
15 Pelvic A_y	
16 Pelvic A_z	
17 Strap Load (on lap belt)	

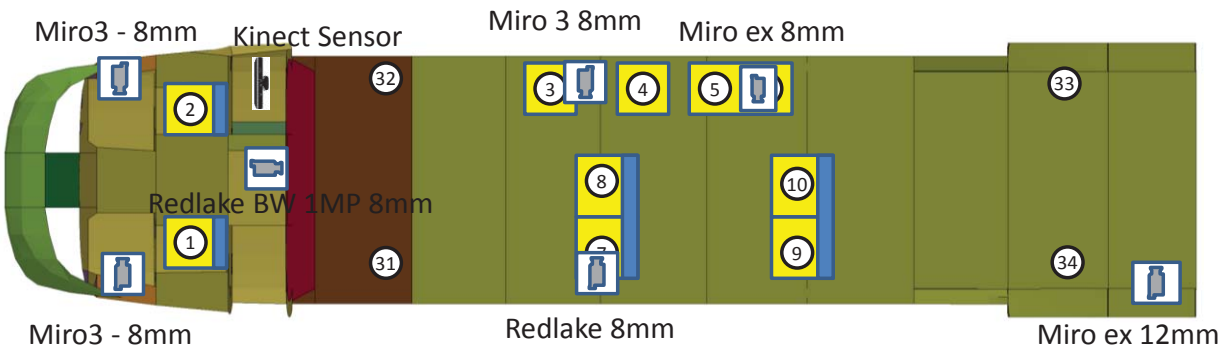

Figure 21. Cabin instrumentation- ATD and high speed camera, top view

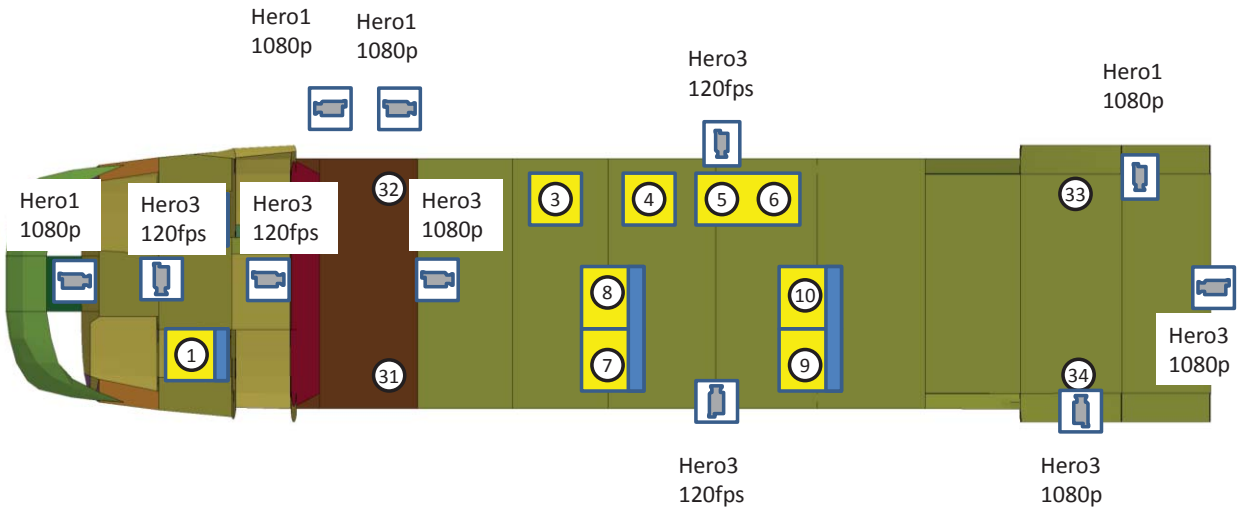

Hero 3 cams film 720 @ 120 fps
Hero 1 cams film 1080p @ 60 fps

Figure 22. Cabin instrumentation ATD and high definition camera- top view

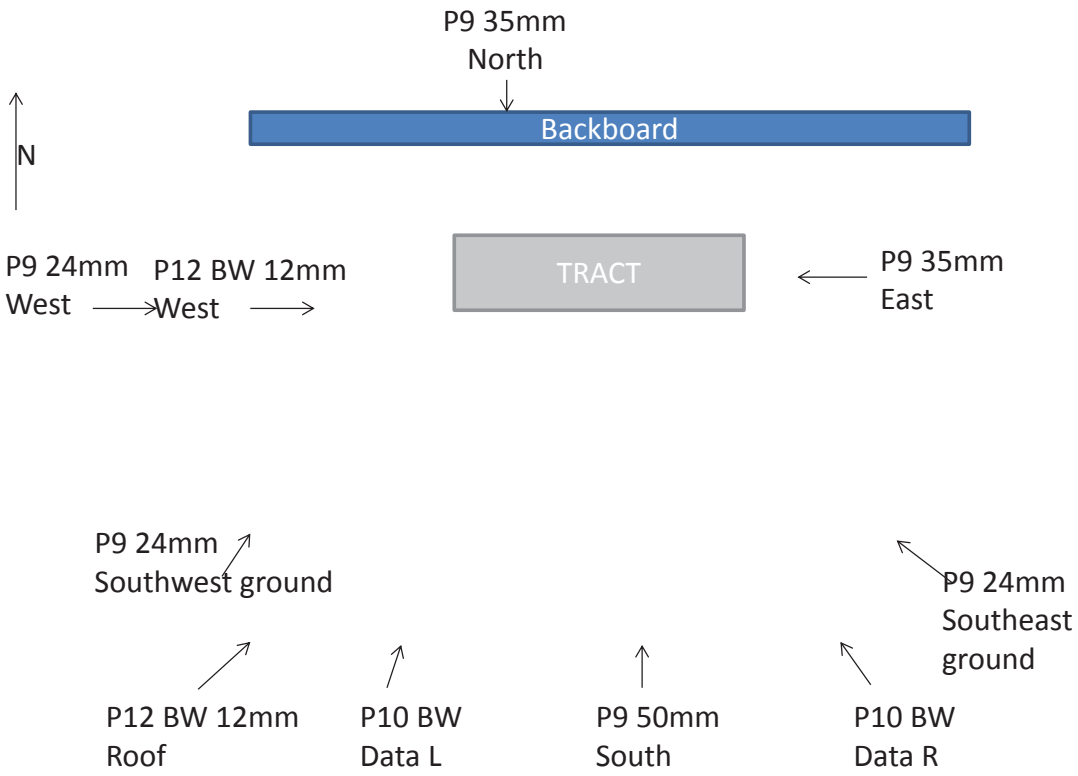

Figure 23. External camera layout

Weight and Balance Data

The locations of the four swing cable and two pullback cable interfaces to the TRACT test article were dependent on the location of the CG. Any misalignment of the cables relative to the CG would cause the test article to pitch and roll upon release, causing a deviation from the intended impact attitude. To verify the predicted weight and balance estimates, the test article was suspended from three cables and pitched up to determine the CG in all three axes, as shown in Figure 24. The fully-loaded, fully-instrumented test article weighed 10,300-lb. The vertical CG was 3 inches above the swing cable and 6 inches above the waterline. The lateral CG was less than 1 inch from the centerline. The longitudinal CG was near FS 260.0. The actual weight and CG location matched well with the estimates.

Figure 24. Photograph taken during weight and balance testing

Impact Conditions

The impact conditions that were defined for the TRACT 1 test are considered to be severe but survivable, based on a survey of mishap data. Figure 25 shows a plot of the 95th percentile velocity change distributions for both civilian and military rotorcraft. The shaded regions pertain to civilian rotorcraft, while the solid lines show boundaries for military design requirements and mishap data. The velocity profiles for military aircraft are much higher than civilian with the inclusion of MIL-STD-1290 qualified rotorcraft. A velocity was chosen that would not extend beyond the civilian envelope. By also taking into account the achievable swing velocities of the LandIR, the vertical and horizontal velocities selected were 26 ft./sec and 35 ft./sec, respectively. A pitch attitude was chosen that would guarantee the test article would impact the surface at a nearly flat or slightly nose-up attitude. The accuracy of the pitch attitude for LandIR full-scale swing testing is ±1 degree. A nose-up attitude of 2 degrees was selected.

Mishap data has also revealed that nearly 75% of mishaps occur on soil terrain or water for both civilian and military rotorcraft. Compared to impact on a prepared surface like concrete, impact on soil would potentially decrease the vehicle vertical deceleration due to soil compliance, but would increase the longitudinal deceleration because of plowing and lesser rebound. Evaluation of the occupant and cargo restraints was predicated on introducing a substantial component of longitudinal deceleration (>10 g). A soil impact surface was chosen that was a combination of sand and clay that had been used previously for land-landing tests of the NASA Orion Crew Module (ref. 13). A soil bed 120-ft. long, 20-ft. wide, and 2-ft. tall was laid on top of the LandIR concrete.

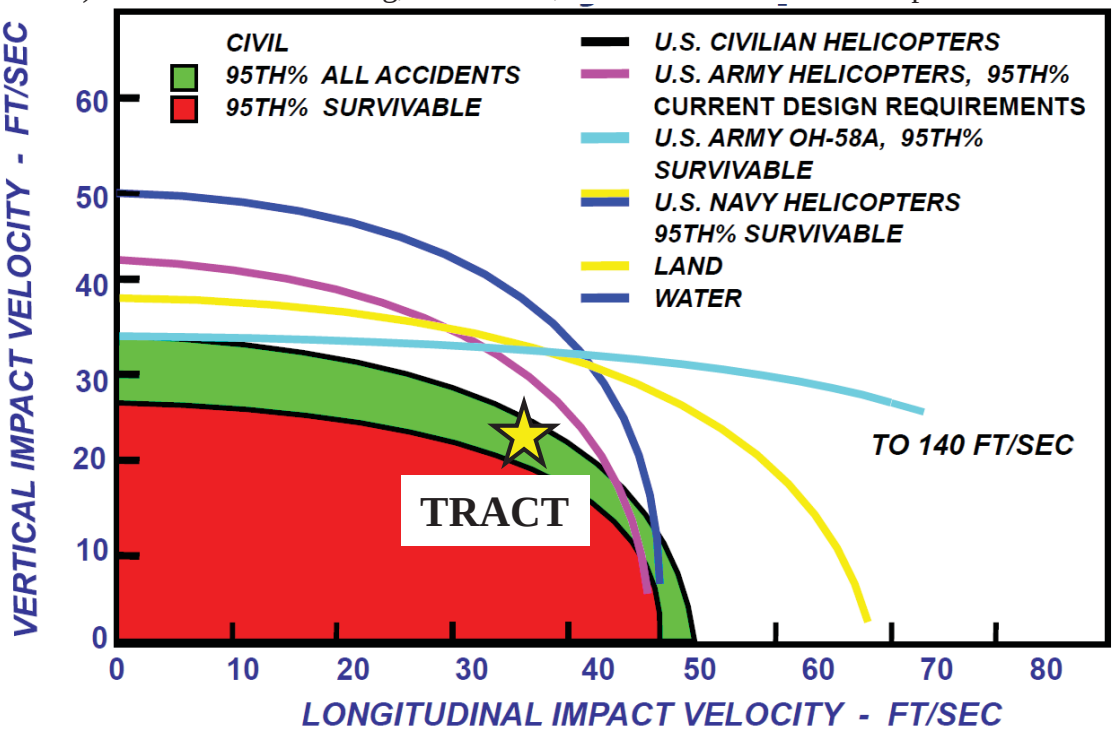

Figure 25. Comparison of civil and military survivable velocities

RESULTS

Pre and Post Test Photographs

Photographs of the TRACT 1 airframe in the release position and just following impact are shown in Figure 26. All external and onboard high speed video cameras properly triggered and recorded data through the swing and impact phase. The actual impact conditions are listed in Table 7. A photo time lapse from an external high-speed camera is shown in Figure 27 and Figure 28. The airframe impacted the soft soil with a 2.5° nose-up pitch attitude, causing the aft frames to impact initially. Next, the airframe rotated allowing the forward cabin to impact the soil. The duration of the point of impact to cockpit contact was approximately 0.020-sec. At 0.1-sec, the helicopter rebounded slightly, while maintaining a slight nose-down pitch and rolling towards the starboard side. A secondary impact occurred at 0.55-seconds, and the test article came to rest at 0.9-sec. The test article slide out was 8 ft.

(a) Pre-test photograph. (b) Post-test photograph.

Figure 26. Pre- and post-test photographs

Table 7. Impact conditions

	Design	Actual
Vertical velocity	26 ft./sec	25-ft/sec
Horizontal velocity	35 ft./sec	33-ft/sec
Pitch	2° nose up	2.5° nose up
Roll	0°	0.5°
Yaw	0°	Less than 1°

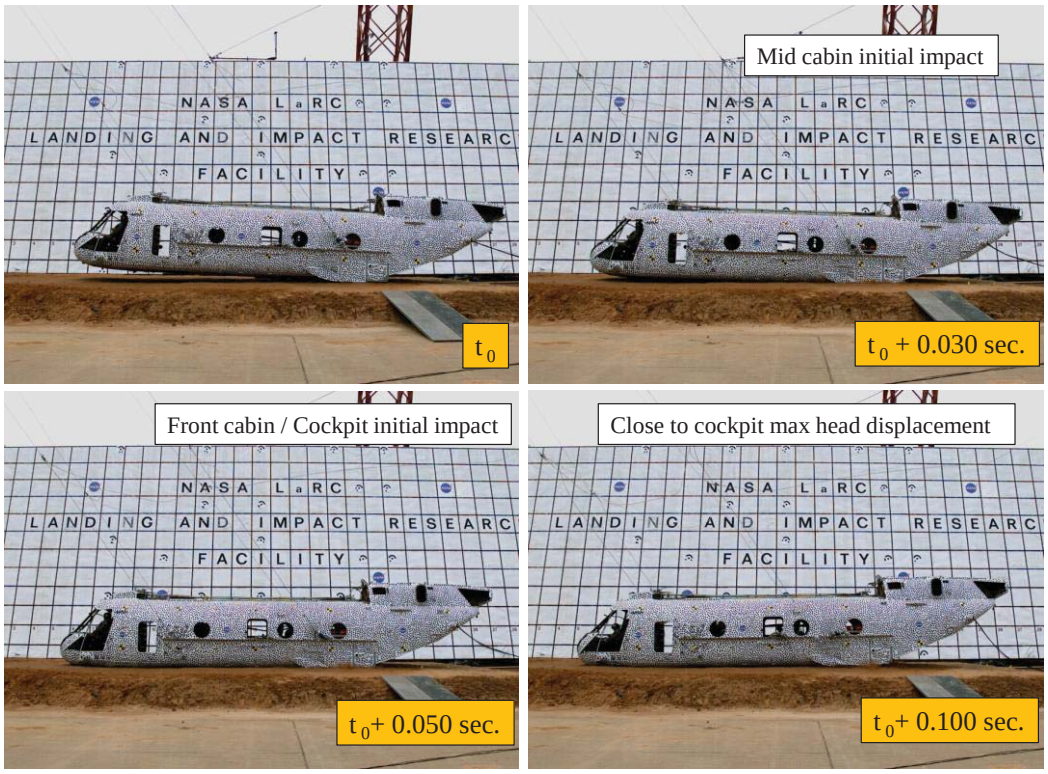

Figure 27. Impact sequence of TRACT I test- 0-0.200 seconds

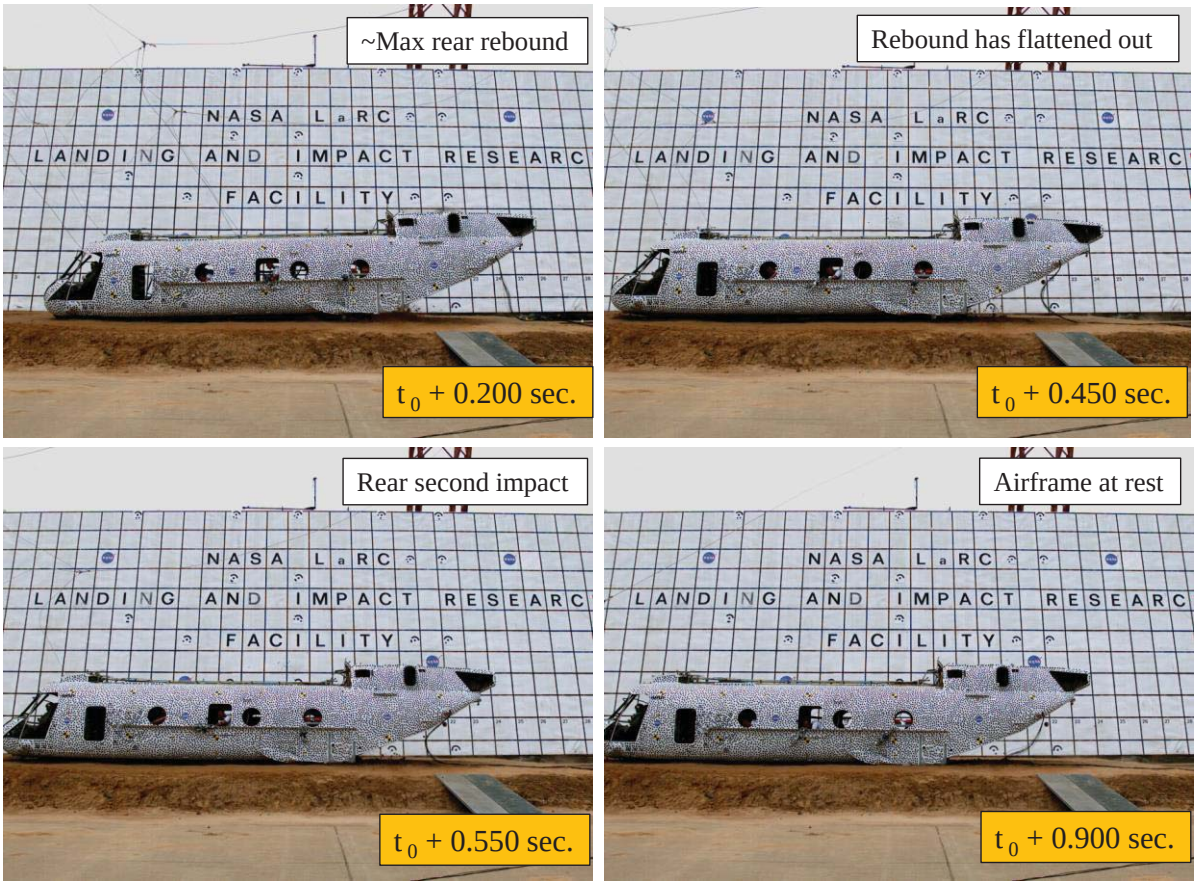

Figure 28. Impact sequence of TRACT I test- 0.200-0.9 seconds

Structural damage to the helicopter was observed in the shear panels located beneath the floor at discrete FS locations. Damage to these panels was more severe near the rear of the aircraft, which is the location of first ground contact. The rear shear panel deformations from FS 320 to FS 410 are shown in Figure 29. Failure modes consisted of plastic deformation, crippling, and tearing. Minor deformation due to longitudinal shear was observed in the shear panels from FS 190 to FS 286 (Figure 30). In addition, some tearing of the material was noted adjacent to rivet lines between the outer skin and fuselage frames. Wrinkling of the outer skin was also observed, as shown in Figure 31, of the skin underneath the cockpit. Minor deformation was evident on the frame sections above the floor aft of FS 286. No damage was evident on the cabin floor.

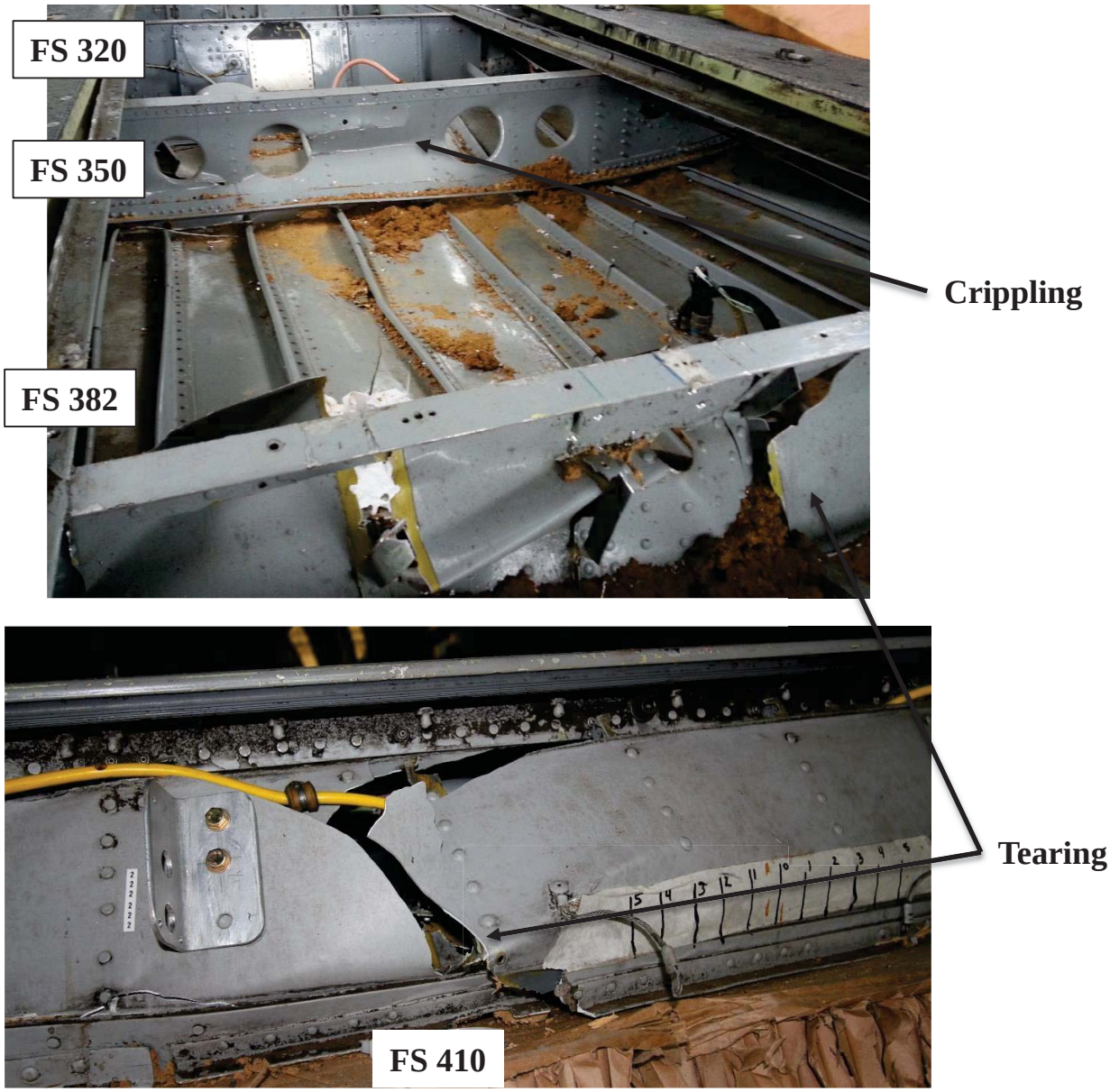

Figure 29. Photograph illustrating failure in rear cabin shear panels

Figure 30. Photograph illustrating failure in mid-cabin shear panels

Figure 31. Photograph illustrating skin wrinkling underneath cockpit

Airframe Time History Results

A schematic of the fuselage highlighting airframe FS locations is shown in Figure 32. All airframe acceleration traces are filtered using an SAE CFC60 filter (ref. 14). It is important to note that FS 410 is located at the aft cabin/tail splice frame, FS 254 is located at mid-cabin, and FS 152 is located at the cockpit/forward cabin splice frame. The pilot and co-pilot responses are recorded on the floor supporting the seat rails.

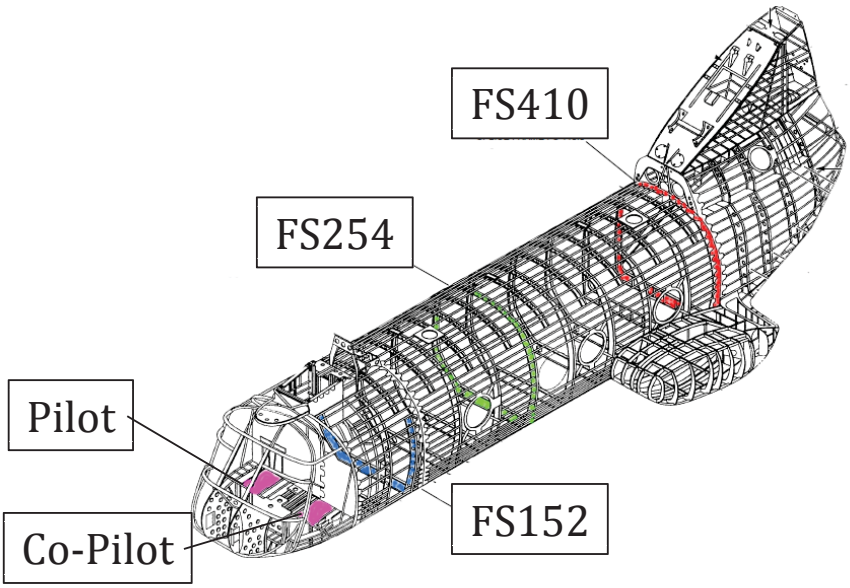

Figure 32. Schematic of helicopter showing instrumentation locations

Given the nose-up pitch attitude at impact, it is expected that the onset of acceleration would occur first for FS 410, next for FS 254, and last from FS 152. The data shown in Figure 33 confirm this expectation. The left side acceleration responses range in peak magnitude between 25- and 45-g with durations of approximately 0.08 seconds. The right side responses range in peak magnitude between 22- and 55-g with a duration of approximately 0.08 seconds. The difference in responses between left and right are attributed to the seat m. At FS 152, there is a noticeable negative component of acceleration before 0.03 seconds as the test article pitches down. The behavior is more pronounced in the pilot and co-pilot responses. The co-pilot and pilot responses have very high magnitude oscillations after slam down at 0.04 seconds. There is a high different between the co-pilot and the pilot responses because of the locations of the accelerometer blocks on the thin-walled floor.

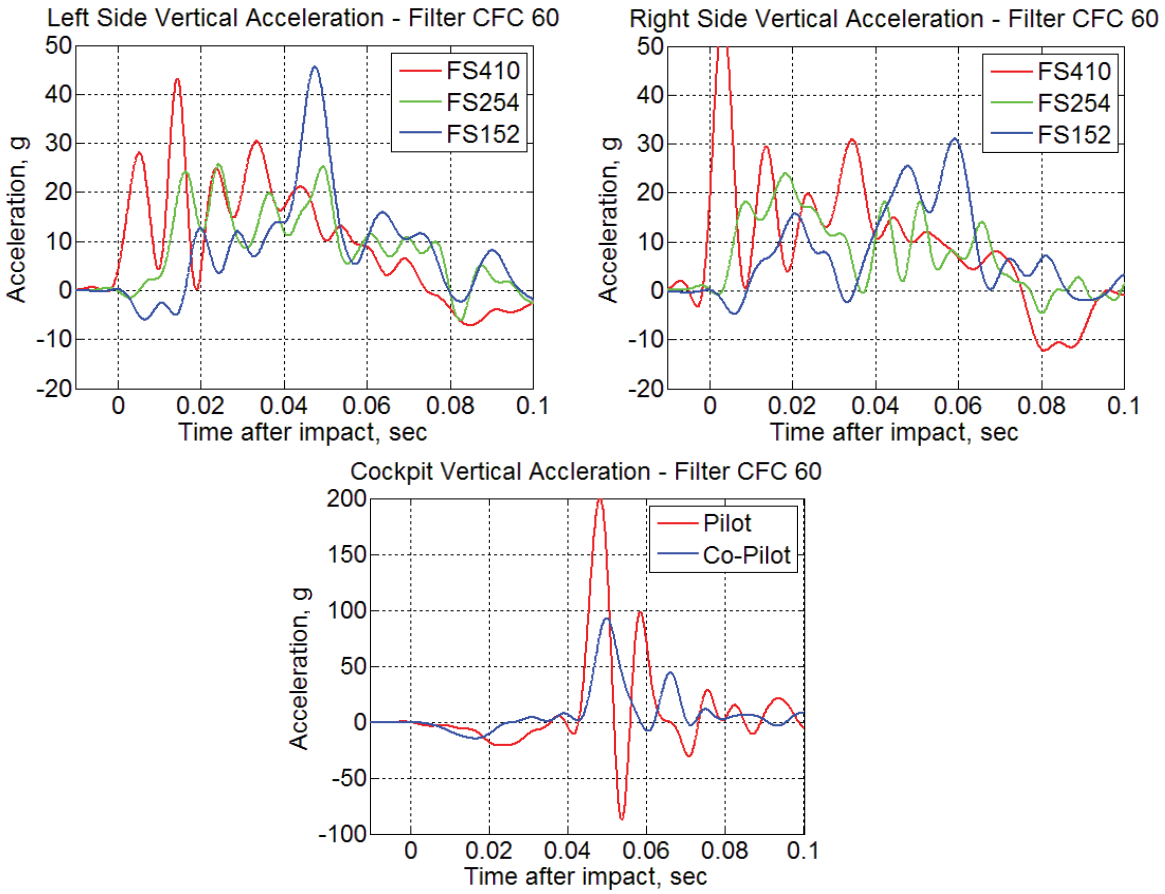

Figure 33. Vertical floor-level acceleration results for the left and right sides of the cabin and the cockpit

Horizontal acceleration time history responses are shown in Figure 34, along with a fuselage schematic showing instrumentation locations. Three plots are shown for the left and right sides of the airframe, and for the cockpit. Each of the curves shows a similar response, with average magnitudes of approximately 10-g. The entire aircraft begins to longitudinally decelerate within the first 0.005 seconds. The magnitude of the peak horizontal acceleration is approximately 30-g; however, most traces are lower.

The orientations and magnitudes of the resultant accelerations just before and after cockpit belly impact are illustrated in Figure 35. In Figure 35a, the orientation of the airframe deceleration is pointed to the aft and down. The pilot and co-pilot excursions are in the opposite direction, upward and forward. The magnitude of the negative component is approximately 10-g during nose over. In Figure 35b, after cockpit belly impact, the acceleration is directed up and slightly aft with a magnitude greater than 95-g.

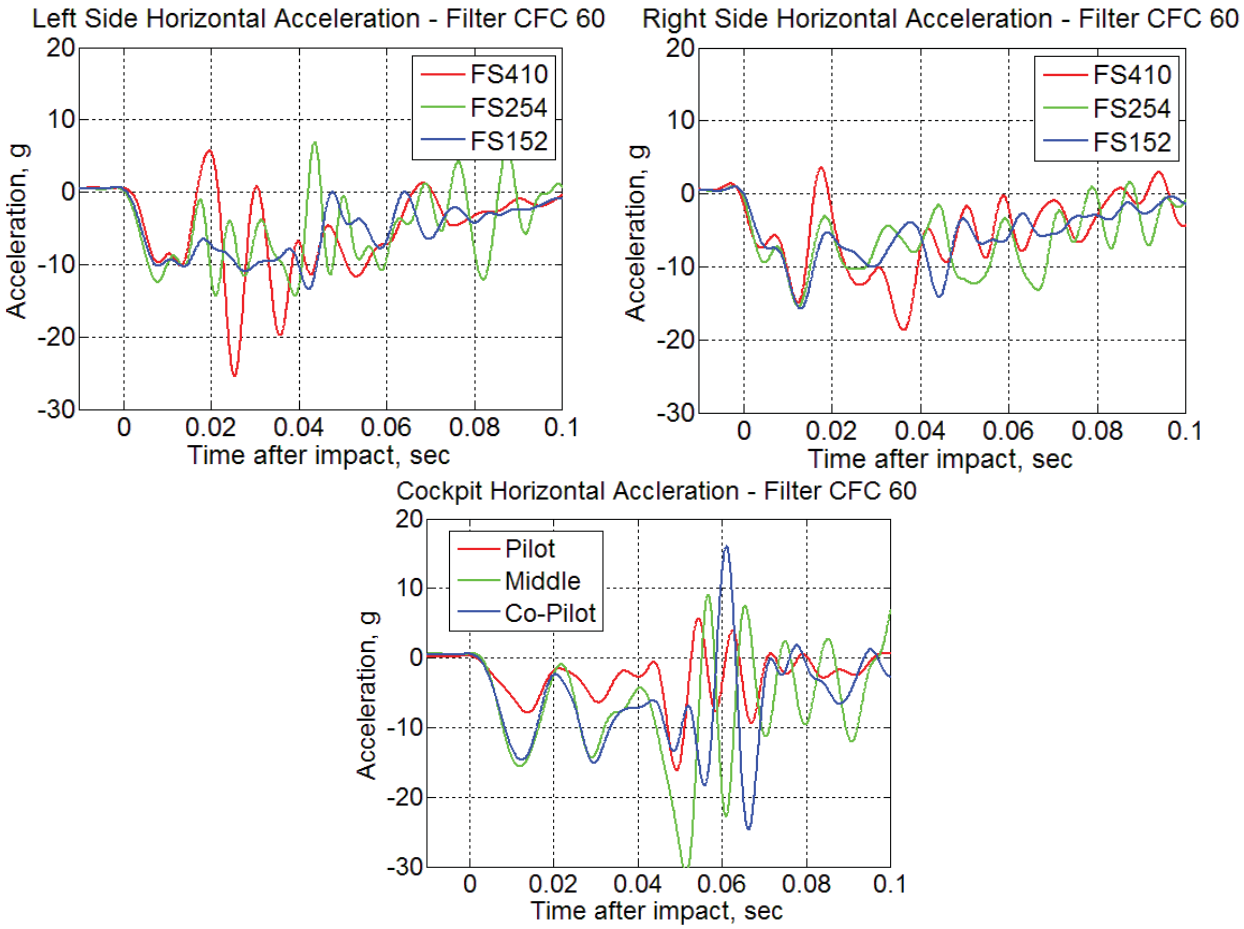

Figure 34. Horizontal floor-level acceleration responses

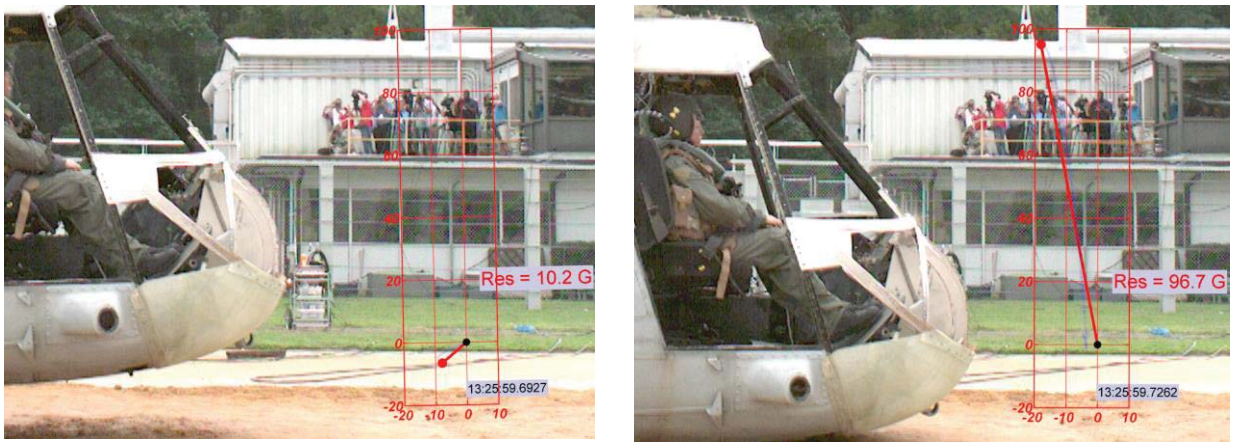

Figure 35. Cockpit resultant acceleration

Cabin mid-wall and floor vertical acceleration responses are shown in Figure 36, along with photographs indicating the locations of instrumentation. The mid-wall traces indicate two peaks, the first having a magnitude of approximately 20-g and the second having a magnitude of 25-g. The floor traces are from the two pair of forward facing seats. Whereas the mid-wall traces were

very similar, the floor traces are opposite to one another. The forward seat exhibits a 15-g uniform acceleration response, which suddenly increases near the end of the pulse to a peak of 38-g. Conversely, the rear seat exhibits an initial peak of 34-g, which is reduced to a relatively uniform 15-g response that decays near the end of the pulse. Both responses have durations of approximately 0.08 seconds.

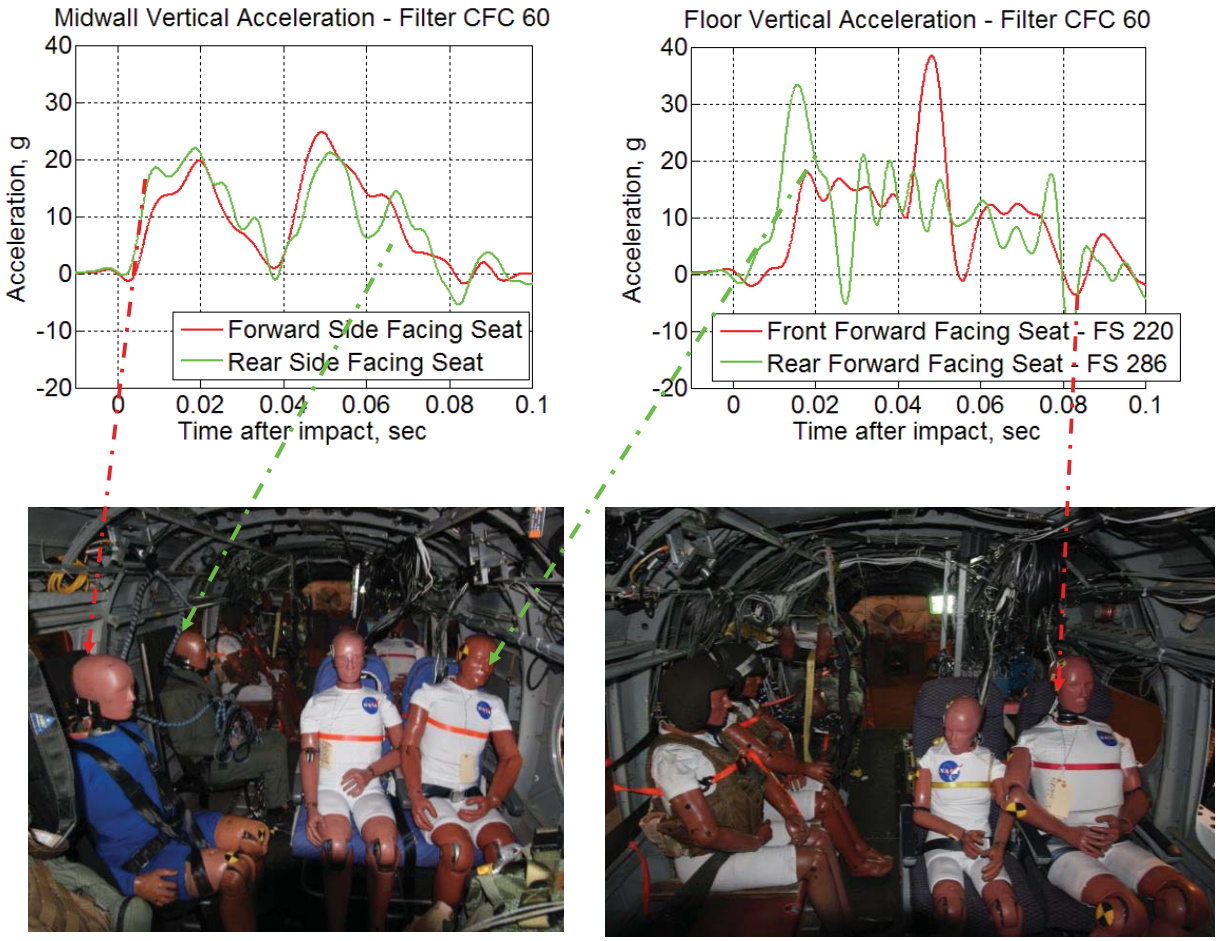

5

Figure 36. Cabin vertical acceleration responses at seat attachment locations

In order to assess the spatial dependency of the accelerometer time histories, a metric proposed by Horta et al (ref. 14) uses singular value decomposition derived basis vectors, or impact shapes. In this approach, time histories from analysis or experiments are decomposed as:

$$y(x,t) = \sum_{i=1}^{n} \sigma_i \phi_i(x) g_i(t) \quad (1)$$

In this form, the impact shape vector ϕ_i sized m x 1 contains the spatial distribution information for m sensors, g(t) contains the time modulation information, σ contains scalar values with shape participation factors, and n is the number of impact shapes to be included in the decomposition, often truncated based on allowable reconstruction error. The fractional contribution of the i^{th} impact shape to the total response is proportional to δ_i, defined as:

$$\delta_i = \frac{\sigma_i}{\sum_{l=1}^{n} \sigma_l} \quad (2)$$

When visualized, the impact shape vectors are also helpful in identifying responses that may be erroneous due to signal corruption, polarity, or sensor mount failure. The impact shapes are plotted by connecting each sensor location with a wireframe. The impact shape mesh and the first three impact shapes are plotted in Figure 37. The first two impact shapes are dominated by cockpit response. The first 10 impact shapes provide 80% of the overall contribution of the response.

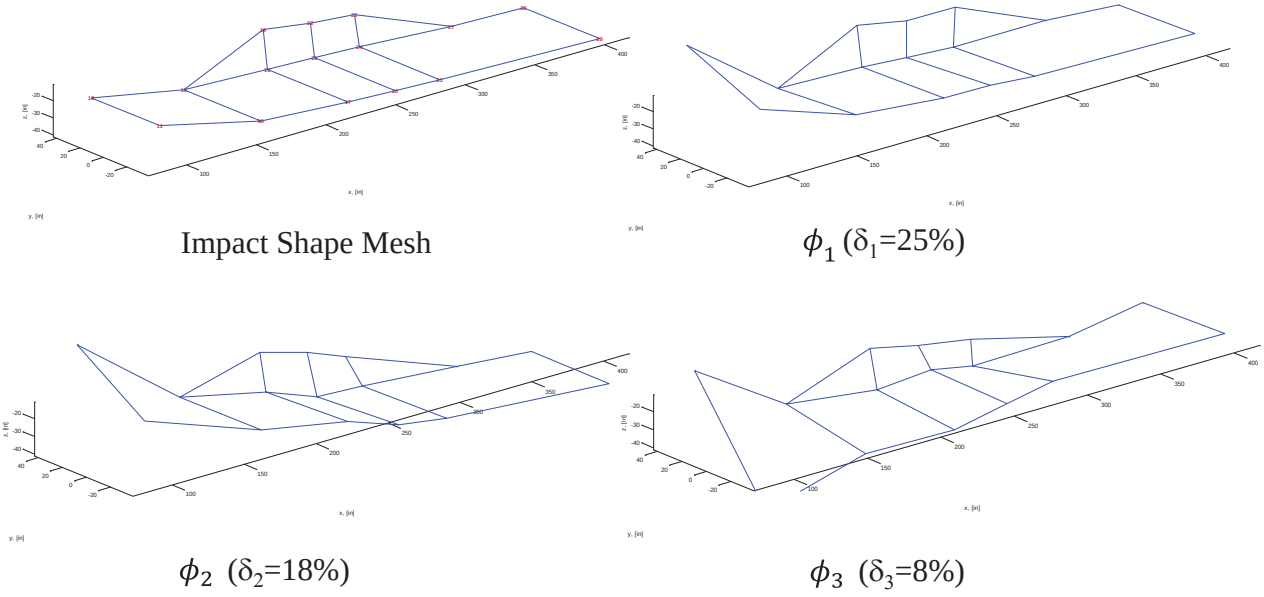

Impact Shape Mesh

ϕ_1 (δ_1=25%)

ϕ_2 (δ_2=18%)

ϕ_3 (δ_3=8%)

Figure 37. Impact shapes from test data

Test Objective 1 Results for CH-46 Crew seat with MA-16 inertia reel and with PARS

A sequence of images from the co-pilot and pilot cameras is shown in Figure 38 and Figure 39. As the rear of the cabin impacts, the PARS system immediately activates and 2-3 inches of webbing retracts within 0.010 seconds. During pitch-over, the pilot and co-pilot ATD excursions are forward and upwards. The feet are lifted off the floor pans, and their buttocks are no longer in contact with the seats. The restraints grab the ATDs and prevent significant excursion. At 0.040 seconds, the cockpit belly impacts and the ATDs re-contact the seat cushions and foot pan.

The seats vertical EAs begin to stroke at 0.080 seconds and the ATDs commence forward flail. Figure 40 shows the lumbar load filtered to SAE Class 600 and vertical pelvic acceleration filtered to SAE Class 1000. Peak lumbar load and vertical pelvic acceleration occur at the time of stroke. Post-test inspection of the seats indicated that the vertical and horizontal EAs stroked approximately 4 inches and 1.5 inches, respectively.

The peak lumbar load is 1,500 lb. for the co-pilot and 2,200 lb. for the pilot, with the duration of loading about 0.060 seconds. While the timing of the EA stroke and motion of the pilot and co-pilot flail are qualitatively consistent, there could be slight differences in motion that would explain the forces. The PARS shoulder belts retracted about 3-4 inches at the point of aft cabin impact, restraining the co-pilot excursion more than the pilot during pitch-over. The altered positions

between pilot and co-pilot when the cockpit belly impacted would have changed the distribution of loading through the lower leg and the pelvis. No tibial load cells were included in the instrumentation; therefore, those loads cannot be differentiated. The current FAA requirement for passenger seats certification is 1,500 lb. for a 50^{th} percentile ATD. This criterion has been reconsidered by the DOD and a lumbar tolerance of 2,065 lb. was recommended (ref. 16). The injury tolerance for the pilot and co-pilot is exceeded based on the FAA requirements, but not the DOD recommendation.

The pelvic acceleration waveforms track the lumbar load similarly. Magnitudes do not track linearly with lumbar load, with magnitude spikes above 70 g for the co-pilot and 100-g for the pilot. These abrupt peaks are caused by the ATD re-contacting the seat pan, and therefore not evident as the load path is damped into the lumbar. The relative velocities between the ATD and seat at the time of re-contact are different from the PARS retraction, causing different dynamic overshoot effects. These accelerations well exceed human acceleration tolerance limits for eyeballs down (+25 g) and would be categorized using Eiband curves as severe (ref. 17). The Dynamic Response Index in the spinal direction (DRIz) is 27.4 for the co-pilot and 30.2 for the pilot, indicating a >50% risk of AIS 2+ injury (ref. 18). These criteria are no longer recognized requirements, and have been superseded by lumbar criteria when evaluating crash loads specifically, but underscore the severe response of the pilot and co-pilot.

The potential for significant neck injury due to axial tension and compression and flexion and extension bending are evaluated by plotting the upper neck axial forces (F_z) and moments (M_y). Maximum neck flexion occurs at approximately 0.120 seconds. The Neck Injury Criteria (Nij) is used to determine the combined effect of axial and bending loads (ref. 19). Kite graphs showing the acceptable limits for force and moment are shown in Figure 41. The time of maximum axial load and bending loads often do not coincide, so Nij is computed for multiple instances during impact. Nij is calculated for four select times for both pilot and co-pilot. For the pilot, all forces and moments are within acceptable limits, while there is one case for the co-pilot where the axial tension is marginal.

T-0.001 sec.

T+0.045 sec.

T+0.085 sec.

T+0.123 sec.

Figure 38. Co-Pilot ATD response

T-0.001 sec.

T+0.045 sec.

T+0.085 sec.

T+0.123 sec.

Figure 39. Pilot ATD response

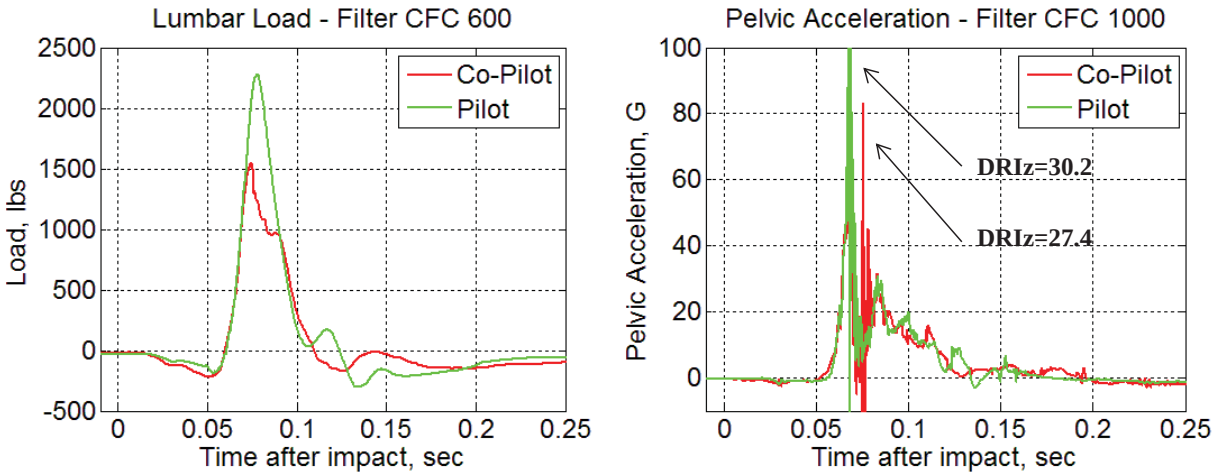

Figure 40. Pilot/Co-pilot ATD lumbar load and vertical pelvic acceleration

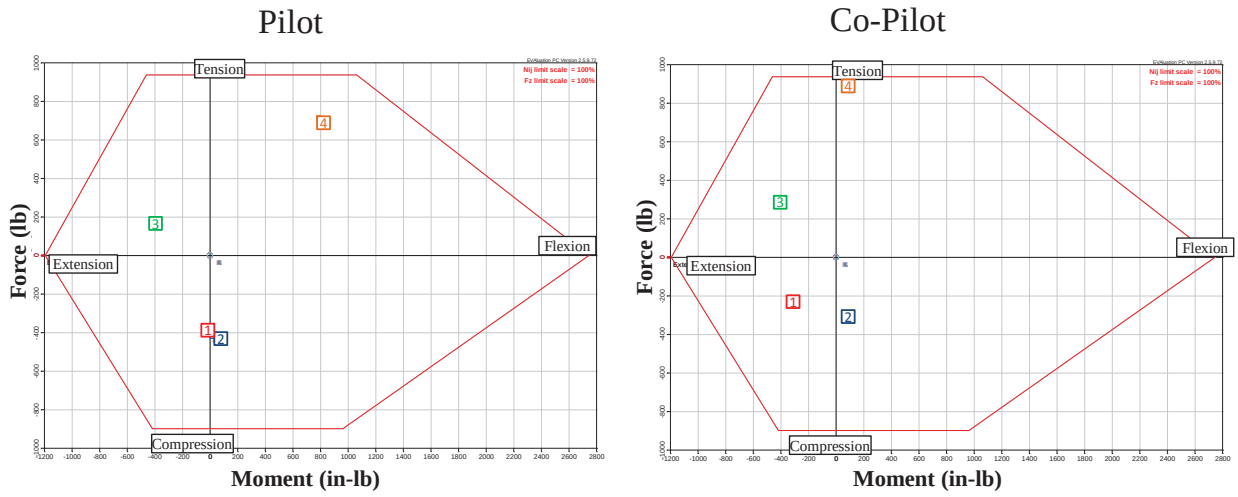

Figure 41. Pilot/ Co-pilot Nij

Test Objective 2 Results for Floor Mounted Passenger ATDs

The sequences of images for the forward facing 50th percentile ATDs and 5th and 95th ATDs are shown in Figure 42 and Figure 43, respectively. The ATDs press into the seat cushions instantly after impact. Neck flexion and torso flail initiate at approximately 0.040 seconds after impact, and the maximum flail occurs at approximately 0.30 seconds. The ATDs rebound at 0.5 seconds, but flail a second time due to the test article rebounding and impacting again.

Lap belt loads for all four ATDs were less than 350 lb. There was no evidence that energy absorption mechanisms, other than seat cushion compression, were actuated during the impact. Post-test inspection revealed no damage to the seat rail interface and insignificant permanent deformation within the seat frame.

The lumbar loads are notably high for all four ATDs. Figure 44 shows the lumbar load for the 50th percentile ATDs. Load waveforms are similar in shape and duration, which is expected given the

similarity in hardware. The peak lumbar load was 2,900 lb. for the 50th FAA Hybrid III and 2,550 lb. for the 50th Hybrid II. The duration of the loading was approximately 0.060 seconds. These lumbar loads are well above the 1,500 lb. FAA limit, and would suggest a high likelihood of severe spinal injury. The peak lumbar load was approximately 1,600 lb. for the 5th Hybrid III and 2,500 lb. for the 95th Hybrid III. The lumbar load for the 5th female is an estimate from the waveform that appears to have saturated. This saturation is actually a scaling error identified post-test that limited the output range for that channel. The peak load of 1,600 lb. was determined through extrapolation. There is not a specific FAA requirement defined for the 5th and 95th ATDs. However, the DOD has recommended injury limits of 1,281 lb. for the 5th female and 2,534 lb. for the 95th male (ref. 14). The DOD recommendations for the 50th ATD are scaled up relative to the FAA requirement. Therefore, equivalent civilian requirements for the 5th and 95th would likely be lower. It is evident that lumbar loads for the 5th female and 95th male are near or above injury tolerance levels as well.

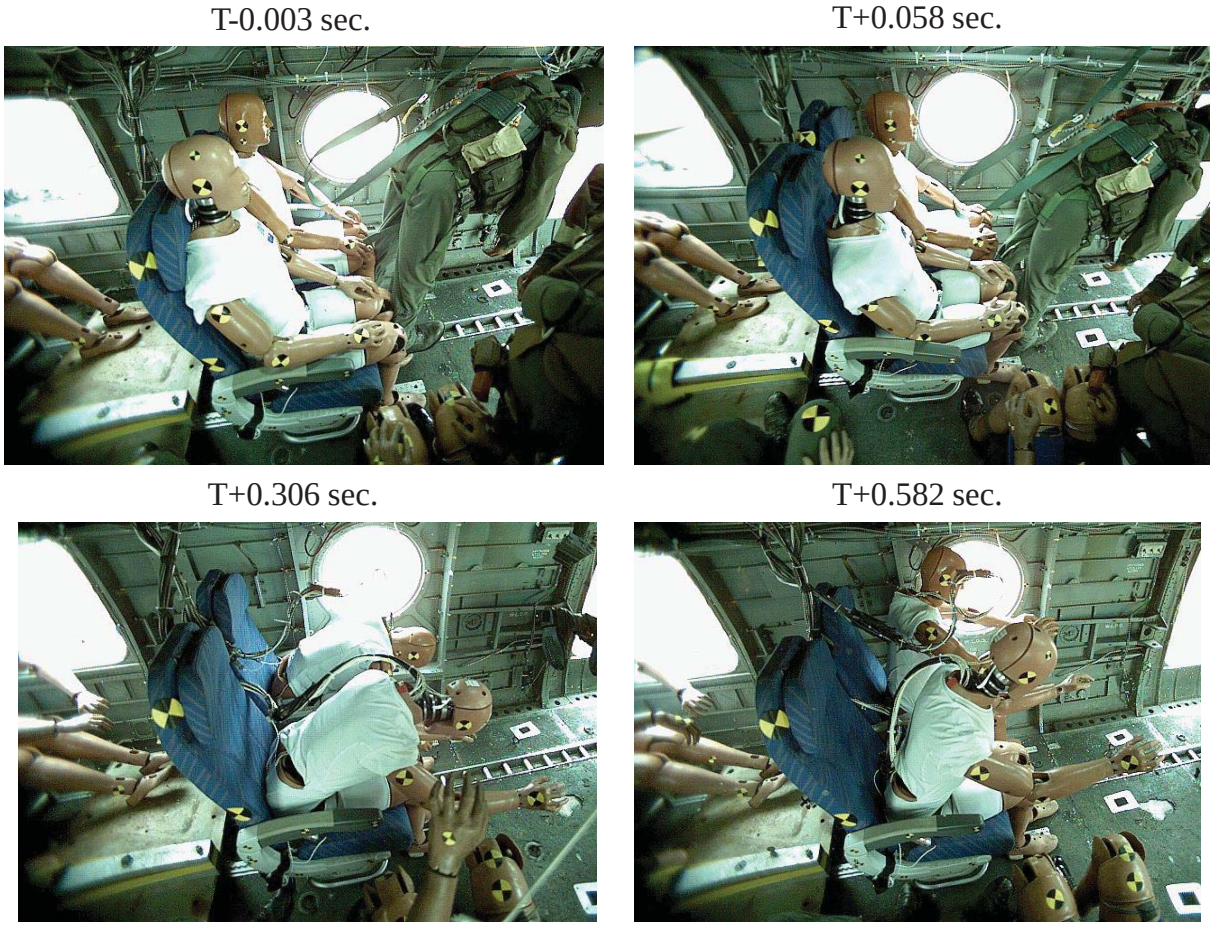

Figure 42. 50th ATDs response

T-0.001 sec.

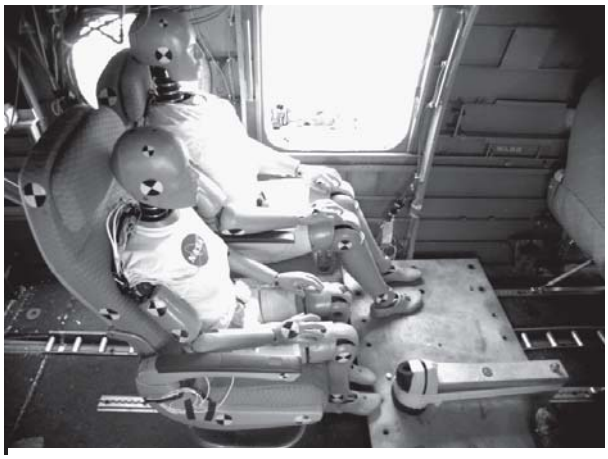

T+0.042 sec.

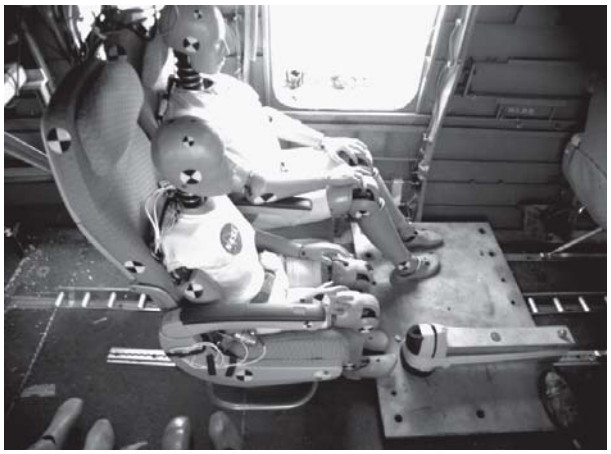

T+0.286 sec.

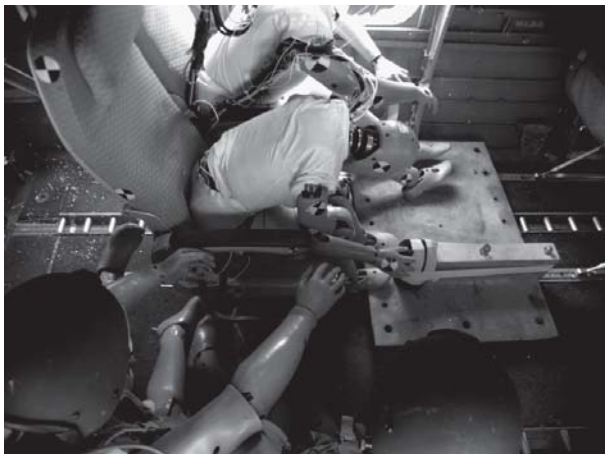

T+0.534 sec.

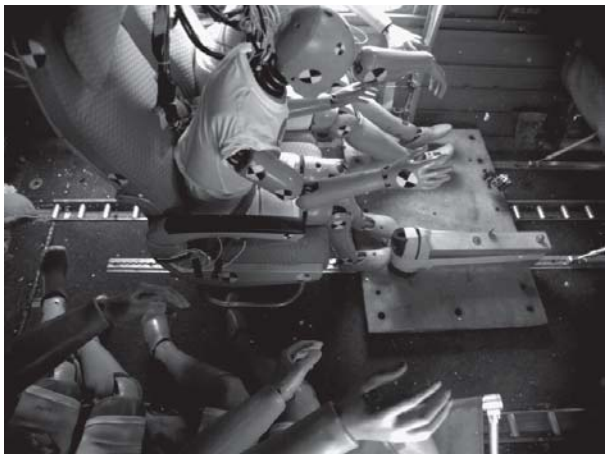

Figure 43. 5th and 95th ATD response

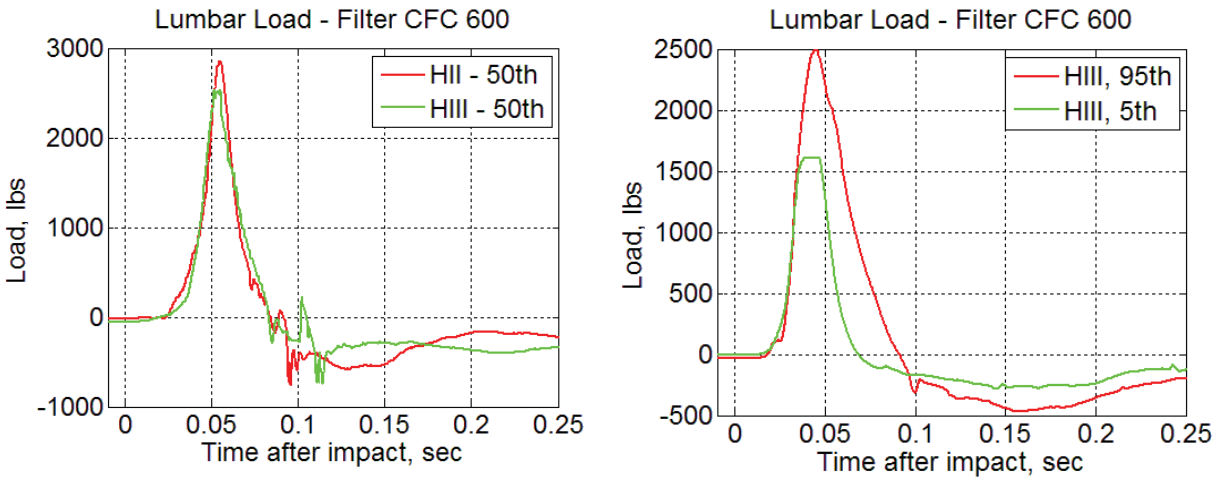

Figure 44. Forward facing ATDs, lumbar load

Test Objective 3 Results for Standing ATD with Gunner's Belt and MARS

The two mobile aircrew surrogates both released simultaneously from their temporary restraints and followed a symmetric trajectory during airframe deceleration to create relative velocity between the ATDs and the airframe. This continued until the ATDs were nearly in a "hands and knees" position on the floor of the airframe. Between steel cable release and the hands and knees position, the MARS locked and webbing payout was restricted. By the time the MARS ATD was in a hands and knees position, the MARS had arrested his vertical excursion toward the fuselage floor and he began to swing forward and up. At the same time, the gunner's belt on the gunner's belt ATD was still slack. The gunner's belt ATD moved right past the hands and knees position to impact the cabin floor followed by a forward slide along the floor. Figure 45 contains a high speed video sequence from the outside of the aircraft showing key points during the crash sequence. Frame 1 is at the time the standing ATDs are released from their steel cable loops. At this point, the aft fuselage has contacted the soil, but the forward fuselage is still pitching down. In Frame 2, the head of the gunner's belt ATD is visible inside the crew door. Frame 2 also represents the initiation of seat stroke for the cockpit occupants. Frame 3 clearly indicates a symmetric response between the gunner's belt and MARS ATDs. The MARS reel has locked at a point between Frames 2 and 3. Also at the time of Frame 3, the cockpit crew seats continue stroking. Frame 4 represents the time of the end of seat stroke for the cockpit occupants. The mobile aircrew ATDs in Frame 4 have symmetrically moved to the 'hands and knees' position. The MARS ATD has continued to move while pulling webbing off of the MARS reel by film spooling (approximately 8- 10 inches.). Frame 4 also indicates that the MARS ATD has started to slow relative to the airframe. Frame 5 depicts a severe contact between the head of the gunner's belt ATD and the floor of the airframe. No such contact has happened with the MARS ATD. Frame 6 shows the gunner's belt ATD sliding forward on the floor and the MARS ATD pulling up away from the floor. Frames 7 and 8 depict the motion of the MARS ATD as he pivots about the MARS.

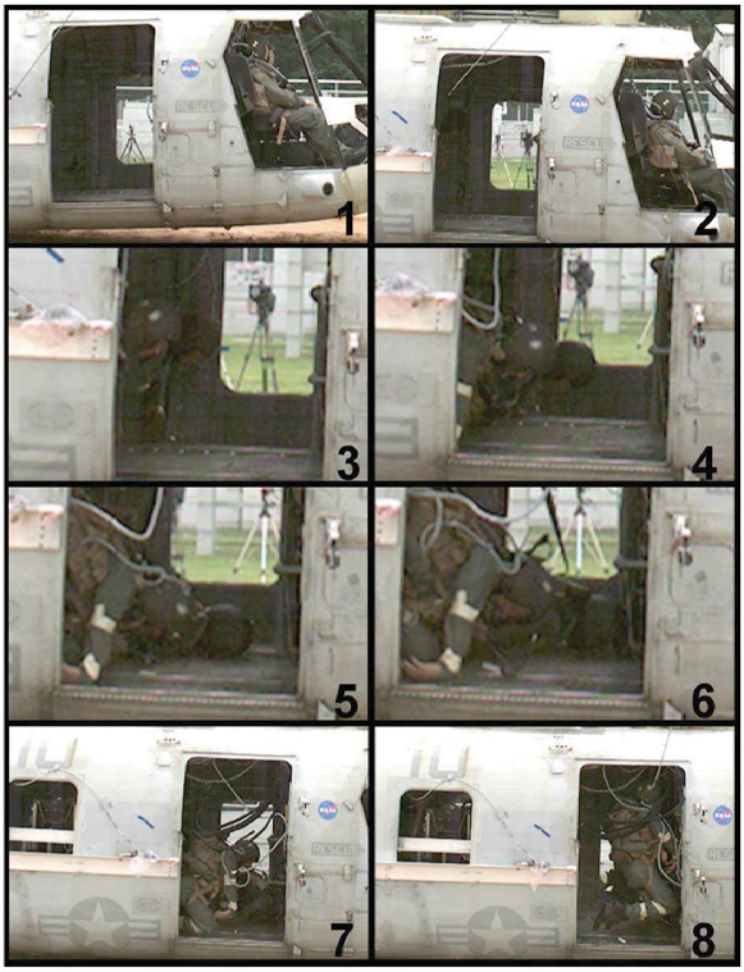

Figure 45. Sequence of mobile aircrew motion during CH-46 airframe crash test.

Figure 46a shows the resultant head acceleration time-histories for both ATDs. The head strike against the floor is clearly identifiable in the acceleration data. Both the magnitude and duration of this head strike are far in excess of human tolerance. With the MARS unit, the strike was prevented and head accelerations are substantially lower and sustained over a much longer duration. Head acceleration measurements indicate the head impact for the ATD with the gunner's belt was a lethal impact. The calculated Head Injury Criterion (HIC) for the gunner's belt ATD was 4,539. Correspondingly, the HIC for the MARS ATD was 248. For reference, HIC values of 1,000 are used as an injury threshold for frontal automotive crash certification, FAA seat performance standards, and Navy qualification test requirements. Figure 46b contains resultant chest acceleration time-histories for the two ATD's. Based on the typical 60-g critical chest acceleration limit, there is again an injurious situation with the gunner's belt ATD and a non-injurious situation with the MARS ATD. Figure 47 shows measured neck forces and moments. Key in these graphs is the remarkable difference between the two ATD's. For all neck forces and moments, the ATD with the MARS experienced less severe loading.

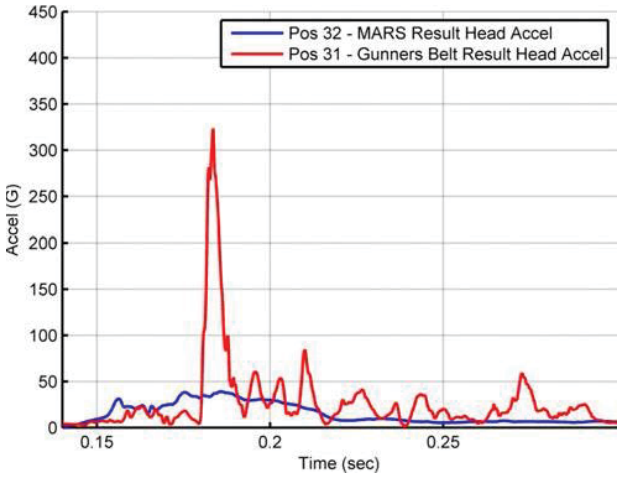

(a) Resultant Head Acceleration

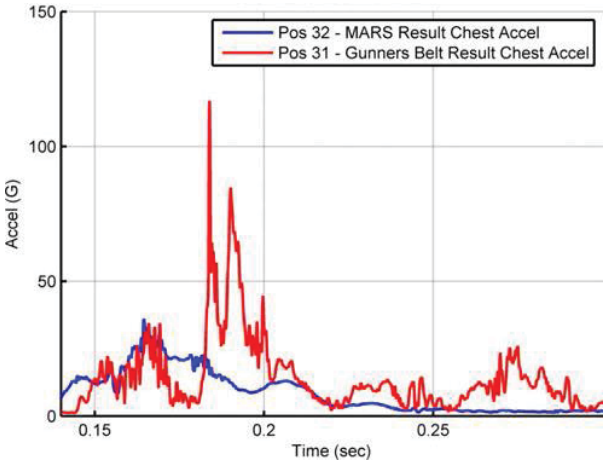

(b) Resultant Chest Acceleration

Figure 46. Resultant Acceleration for Mobile Aircrew ATDs

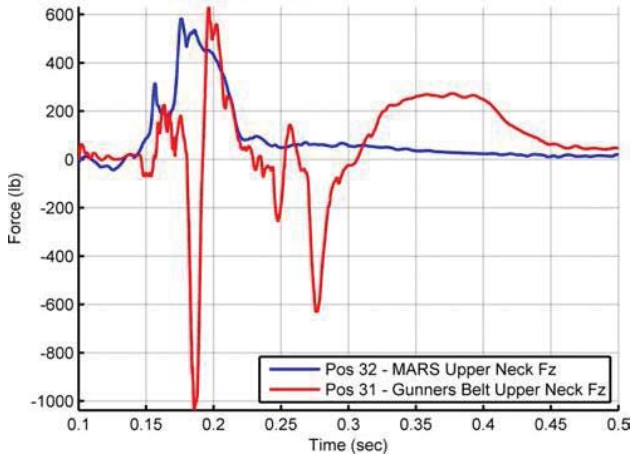

(a) Upper Neck Fz

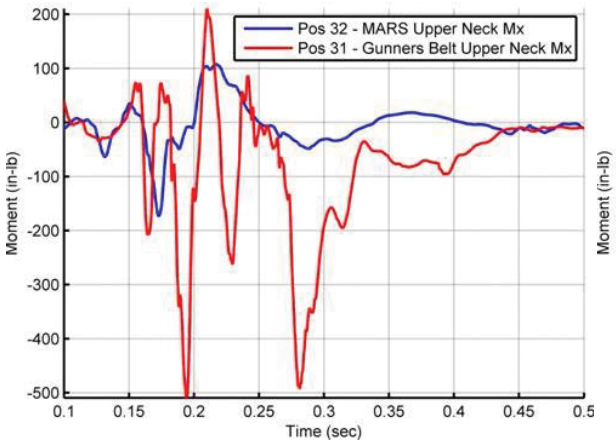

(b) Upper Neck Mx

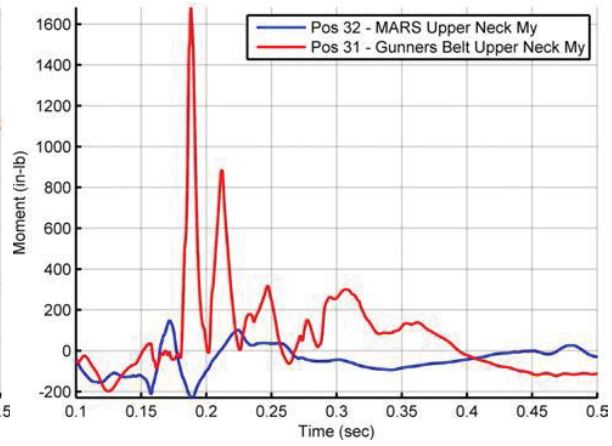

(c) Upper Neck My

Figure 47. Neck Forces and Moments for Mobile Aircrew ATDs

Test Objective 4 Results for Full-Field Photogrammetry

The exterior photogrammetry data was captured and analyzed post-test. Data was computed such that a data point was acquired every 1.5 inches over the entire port side skin of the test article, with over 8,000 data points acquired. A sequence of photogrammetry data that were collected during the crash test is shown in Figure 48. The diagonal regions in which no data are shown are attributed to exterior cables, which obscure the dots.

This displacement starts near the stub wing when this location comes in contact with the ground. As the point of impact of the test article moves forward during the impact, the computed out of plane motion also moves forward. These plots indicate flexing of the fuselage upon impact with the maximum out-of-plane (z) displacement of greater than 1 inch seen in the region of the middle round window above the swing beam between FS 286.0 and 320.0. Finally, the photogrammetric data show areas of permanent deformation around the stub wing locations and lower parts of the skin, near the floor. These locations match areas of damage seen in the fuselage post-test inspections taking the form of skin wrinkling and buckling. Figure 49 shows the discrete time histories of the out-of-plane points at WL +13. These points are interrogated further because the WL +13 points have the highest-on-average out-of-plane displacement. Figure 49 also shows vertical displacements taken from these same points at WL +44, which are the highest-on-average vertical values. These plots, taken together, suggest approximately 0.050 seconds after the impact shows the greatest fuselage deformation.

Further evidence of this flexing is demonstrated in Figure 50. Vertical relative deformation is evaluated by interrogating relative position change between discrete points along the length of the cabin at the frame locations. Five locations were investigated further using this technique. The analysis calculates the maximum change in length of a created line endpoint positions, divided by the original undeformed line length, and reported as a percentage similar to strain calculations. The maximum relative deformation occurs in the front and mid cabin suggesting that the largest unsupported test article locations are those with the highest deformation.

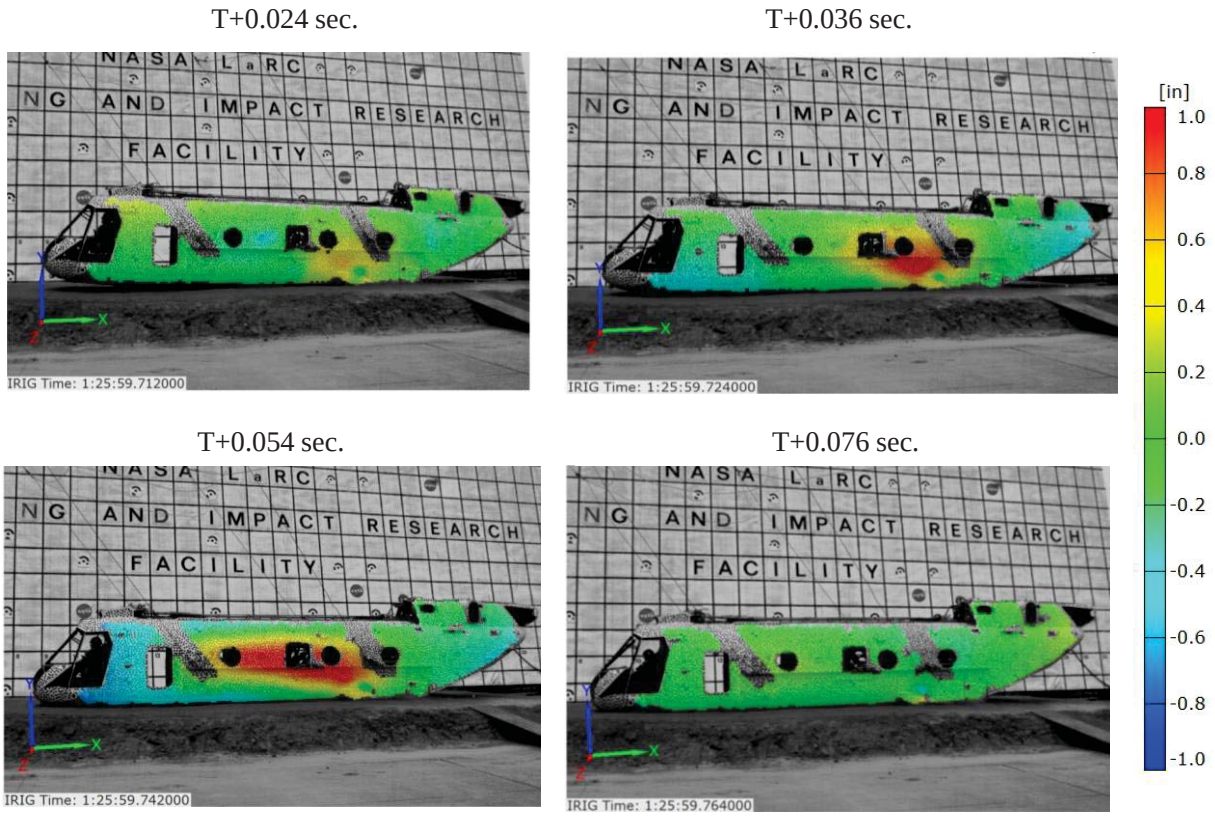

Figure 48. Measured out of plane displacement photogrammetry data

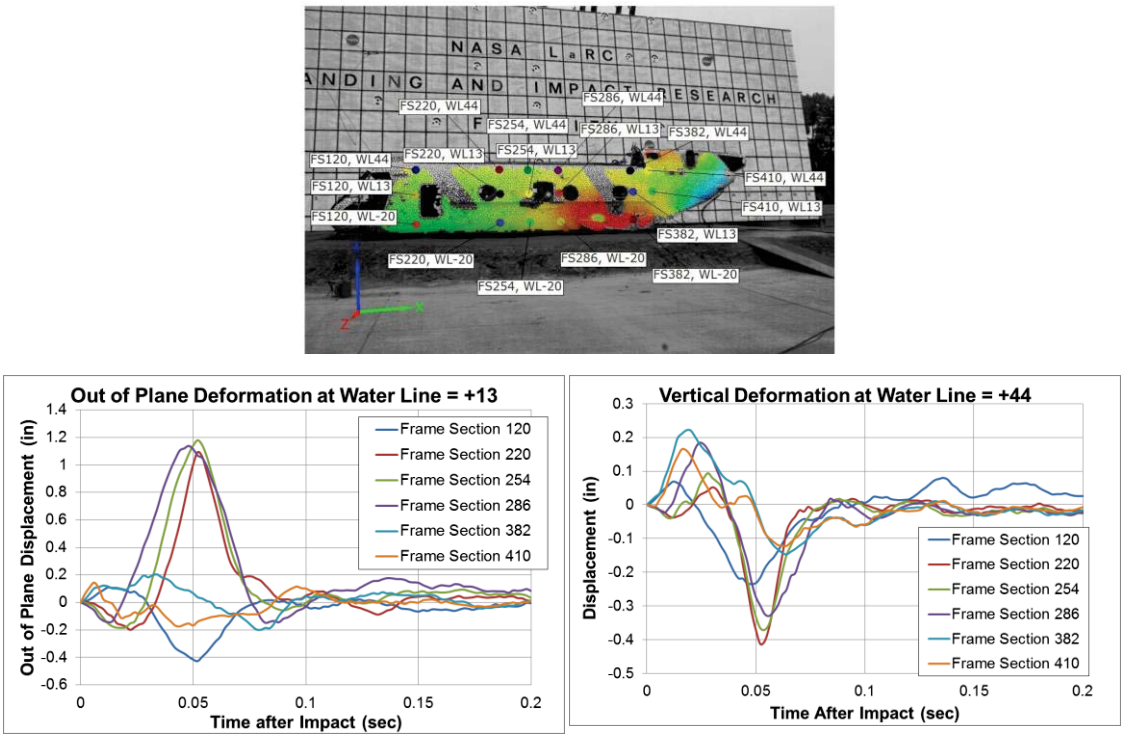

Figure 49. Discrete point time-histories

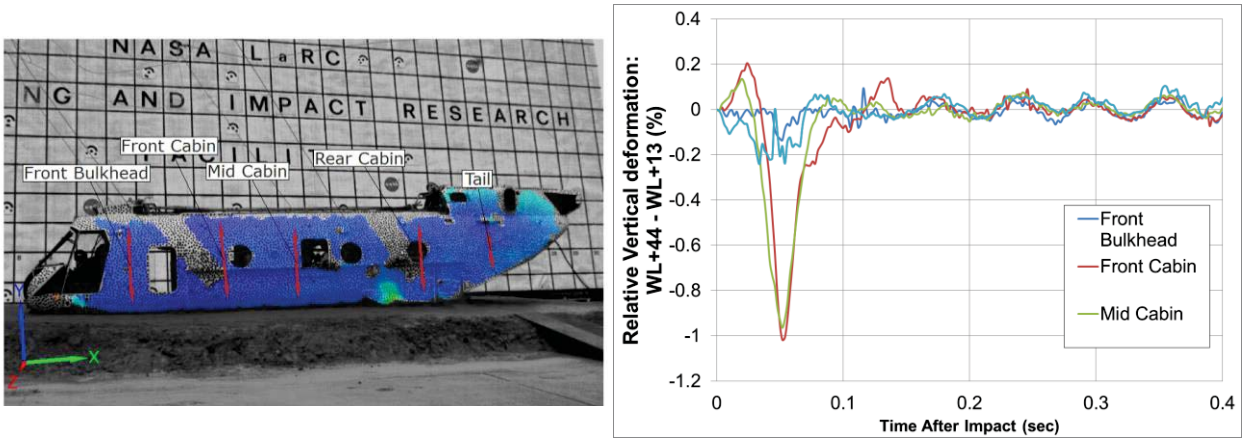

Figure 50. Relative vertical deformation photogrammetry data

Test Objective 5 Results for Sidewall Mounted Troop Seats

A sequence of images from the high speed camera aimed at the CACS side facing ATDs is shown in Figure 51. The ATDs began slumping into the seat bottoms at the point of impact. Vertical stroking of the seat EAs and head lateral rotation started just after 0.050 seconds. The peak head lateral bending occurs at 0.143 seconds, with higher rotation for the ES-2re head compared to the Hybrid III head. Both upper legs of the FAA Hybrid III shifted forward during the impact, twisting the body about the Z-axis. The feet of this ATD remained near their initial position during the impact. The Aerospace Hybrid-III's entire right leg flailed forward, but the left upper leg was restrained from forward motion by the crotch strap of the 5-point restraint. This kept the torso of the ATD in its initial position, exhibiting very little Z-axis rotation. As the ATDs rebounded from maximum head lateral bending, the FAA Hybrid III returned to a side-facing orientation but the right upper leg of the Aerospace Hybrid III remained in the extended position. This difference in leg flail and body Z-axis rotation may be related to the restriction of hip rotation produced by interaction between the ATD femur and the fixed pelvis flesh of the FAA Hybrid III.

Lumbar load and vertical pelvic acceleration are plotted in Figure 52. Examination of the midwall acceleration near each seat (Figure 36) indicates that the aft seat was loaded just prior to the forward seat. If the lumbar load data is overlaid with this time difference removed (a 0.010 second phase shift), it becomes apparent that the onset rate and overall response are very similar. The lumbar load peaked at approximately 1,000 lb. for both ATDs, and pelvic acceleration were limited to roughly 20 g. These loads are regarded as moderate in severity. The total stroke for each CACS seat was noticeably different. The seat with the ES-2re ATD stroked 4 inches and the seat with the Hybrid III ATD stroked 1.2 inches. The load drop exhibited in both cases is evidence that some energy was absorbed by both seats. The larger force drop in the forward seat correlates to the longer stroke observed. The difference in seat stroke may be related to factors such as the loading and unloading behavior of the ATDs, variability in the stroking force produced by each seat's energy absorbers, or interaction with the standing ATD that had moved back against the forward seat occupant after release. Of note is that both seats limited spinal loads (as intended) even though the vertical component of the acceleration pulse applied to them at the sidewall interface was very

different from the idealized triangular shaped pulse applied in dynamic tests to qualify seats of this type (Figure 53).

The differences in stiffness for the ES-2re and Hybrid III necks are evident when comparing ATD upper neck forces and moments, as seen in Figure 54. Axial force and lateral bending moments were 50% lower for the ES-2re neck than the Hybrid III neck. The all of the loads measured at the ES-2re upper neck were well below the force and moment limits cited in the side-facing occupant neck injury criteria recently established by the FAA. These criteria include 405 lb. tension and compression, 185 lb. lateral shear, and 1,018 in-lb. lateral bending moment.

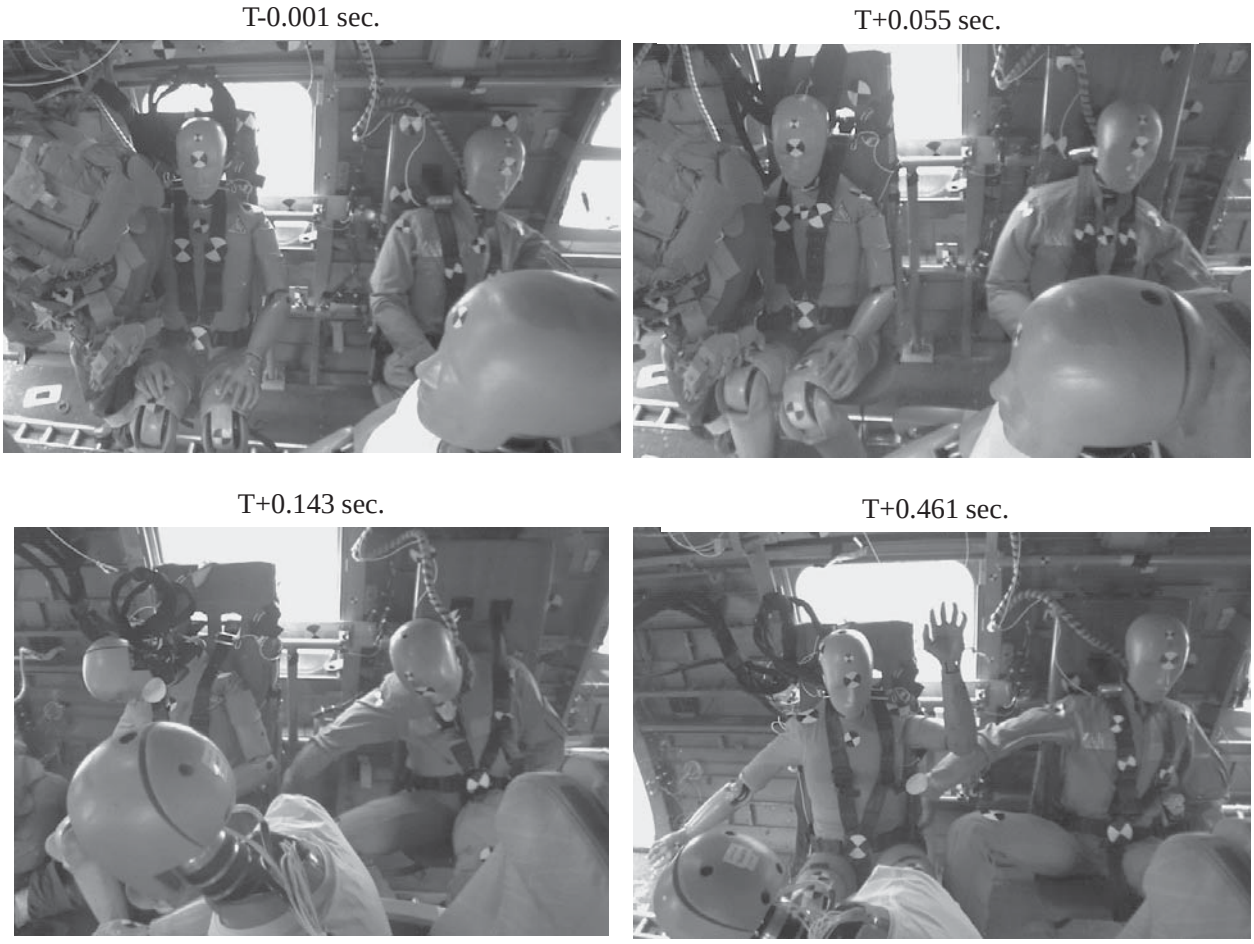

Figure 51. Response of side facing ATDs on CACS

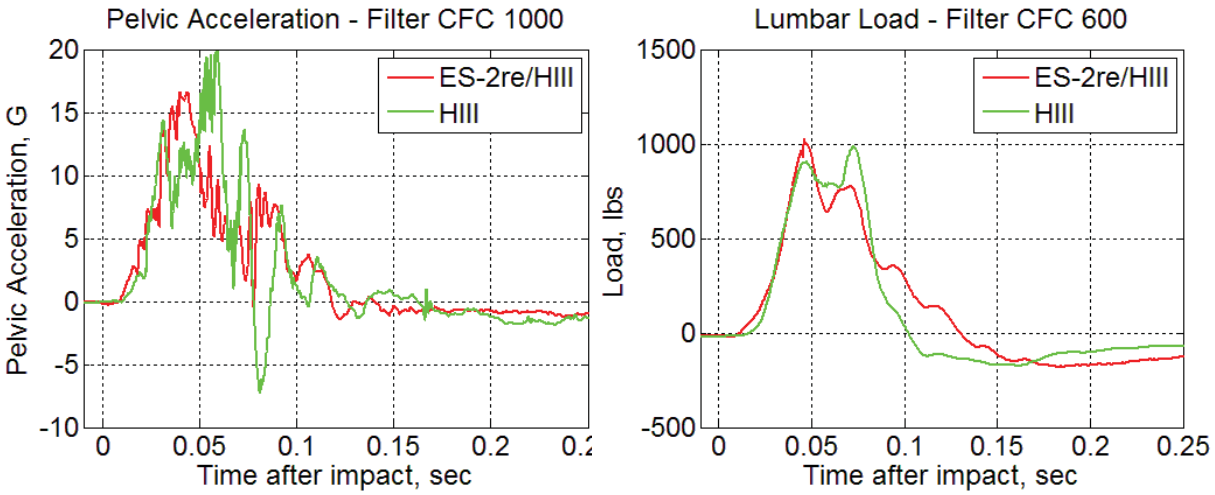

Figure 52. Side facing ATDs on CACS, pelvic acceleration and lumbar load (HIII offset by 0.010 seconds)

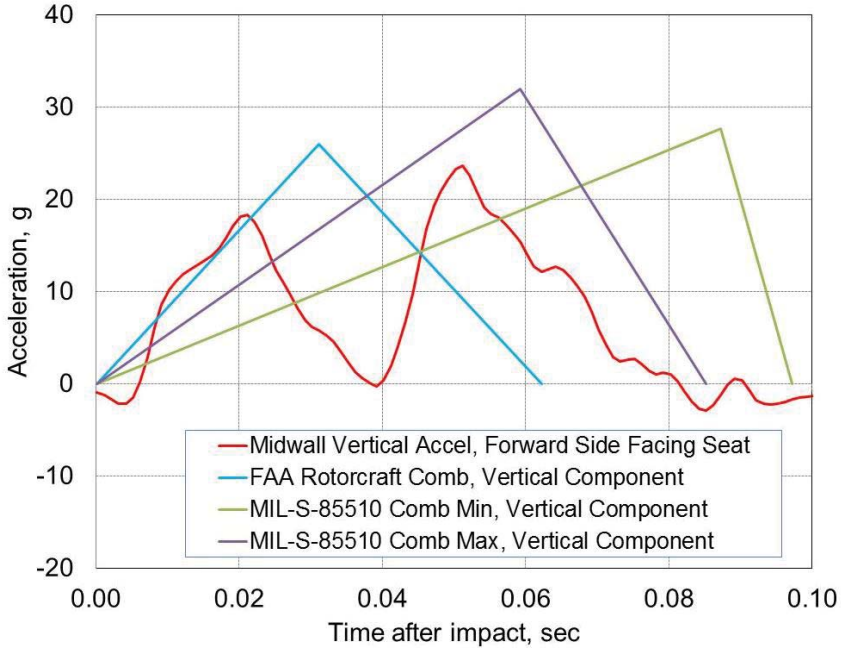

Figure 53. Comparison of sidewall acceleration pulses

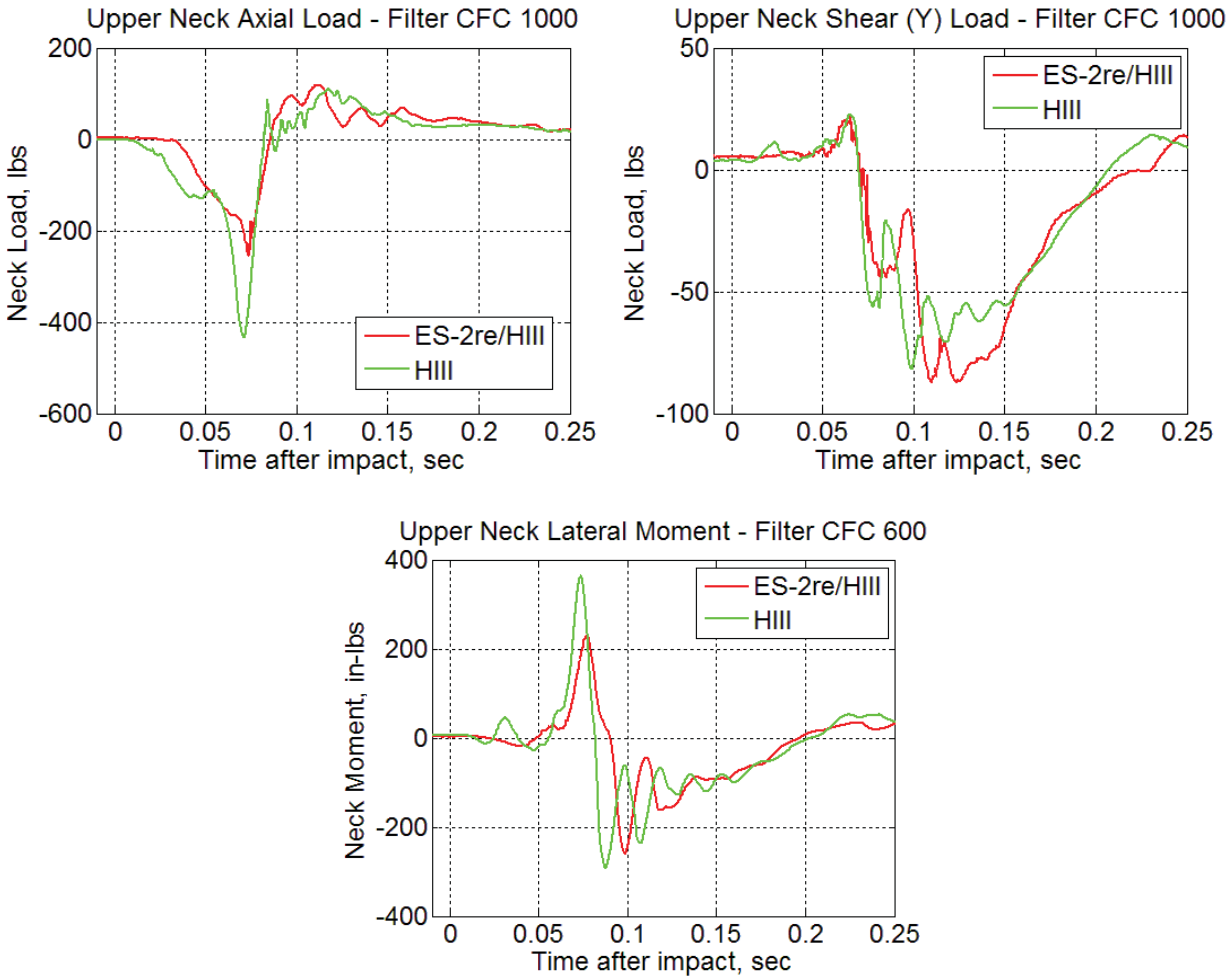

Figure 54. Side facing ATDs on CACS, upper neck forces and moments

The high definition camera aimed at the Hybrid II ATDs on the CH-46 troop bench shifted during impact, and was unable to capture video coverage of the ATD motion. Post-test photos (Figure 55) showed that the seat fabric was torn off the aft frame, the front frame buckled near its center, and the right frame member detached from the aft frame. Because of the seat collapse, evaluation of lumbar load for injury is not appropriate, with more upper leg contact forces than pelvic. The ATD pelvises and upper legs were wedged within the frames, indicating a high likelihood of upper leg injury. Abdominal injury was also possible since the lap belt angle changed.

Figure 55. Side Facing ATDs on troop bench

Test Objective 6 Results for Markerless Tracking of ATD

A limited number of frames of ATD motion were captured using the markerless tracking system. This result is partially due to its low acquisition rate of 30 frames per second, but primarily due to the foot of the standing ATD impacting and dislodging the sensor from its mount during the impact. This impact caused the sensor to break free of its mounted location and become settled on the floor of the airframe, pointed down toward a linkage. However, approximately 62 frames of color and depth images were captured during the free fall prior to impact. The time history in Figure 56 shows a summary of the data captured during the test. Each pair of images contains data from the color sensor, which is presented on the left, and a fringe plot reconstruction of the depth data, which is presented on the right. Since data were unavailable post-impact, the data presented occurs at four different states prior to impact. The depth data shows a graphic representation of ATD distance from the sensor, displayed in units of millimeters (mm). At pre-release, the majority of the ATD is colored green and blue, which represents 1,300 (blue) to 1,700 (green) mm position away from the sensor. The frame prior to impact, labeled pre-impact, shows the ATD is partly green, but primarily red in color. This data suggests that the ATD is between 1,700 and 2,200 mm away from the sensor, representing a half meter change in position away from the sensor from release to impact.

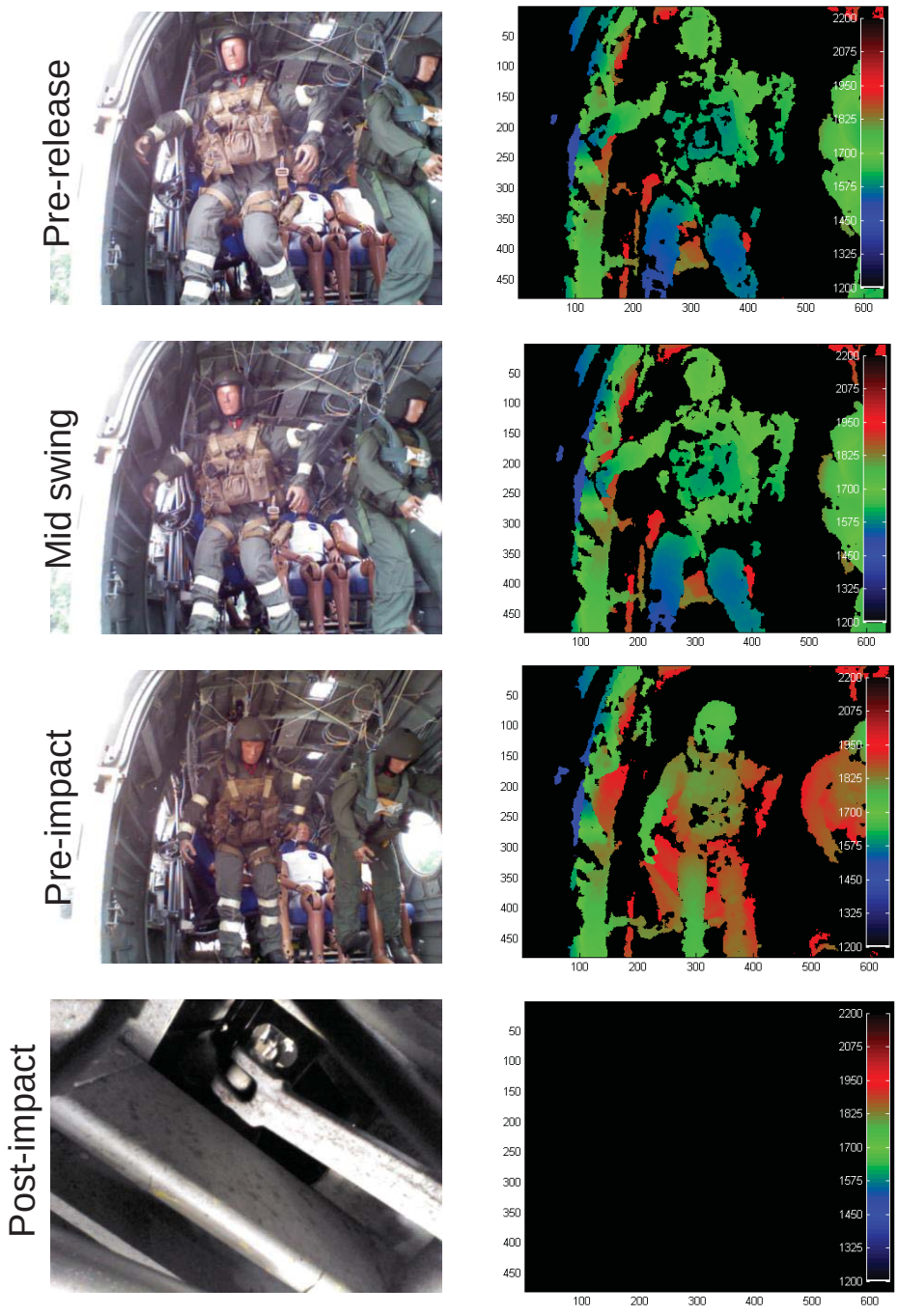

Figure 56. Markerless tracking time history-color image (left) and depth fringe plot (right)

The skeletal tracking algorithms did not associate with the depth data, and therefore, skeletal data was not acquired. Two potential reasons are presented to explain the lack of skeletal capture. The first reason was the shape of the standing ATD. The standing ATD contained a helmet, flight vest, and other various straps and articles which would cause confusion in the tracking algorithms. This theory was proven, when, during a preliminary test, this equipment was removed and the sensor was able to associate a skeletal wireframe with the standing ATD, as shown in yellow in Figure

57. The second reason was a potential interference of the projected dot field due to the outdoor environment. Preliminary testing showed the infrared light generated from the sun had the potential to overlap the projected infrared dot field, essentially washing out the dots and obscuring the measurements. Large holes in the spatial data on the ATD are evident in Figure 56, presumably from this phenomenon. Unfortunately, the placement of the sensor could not be changed due to the high density of experiments on the test article. The position chosen behind the front bulkhead near the floor was the only acceptable location to locate the sensor for ATD tracking and to not interfere with other experiments.

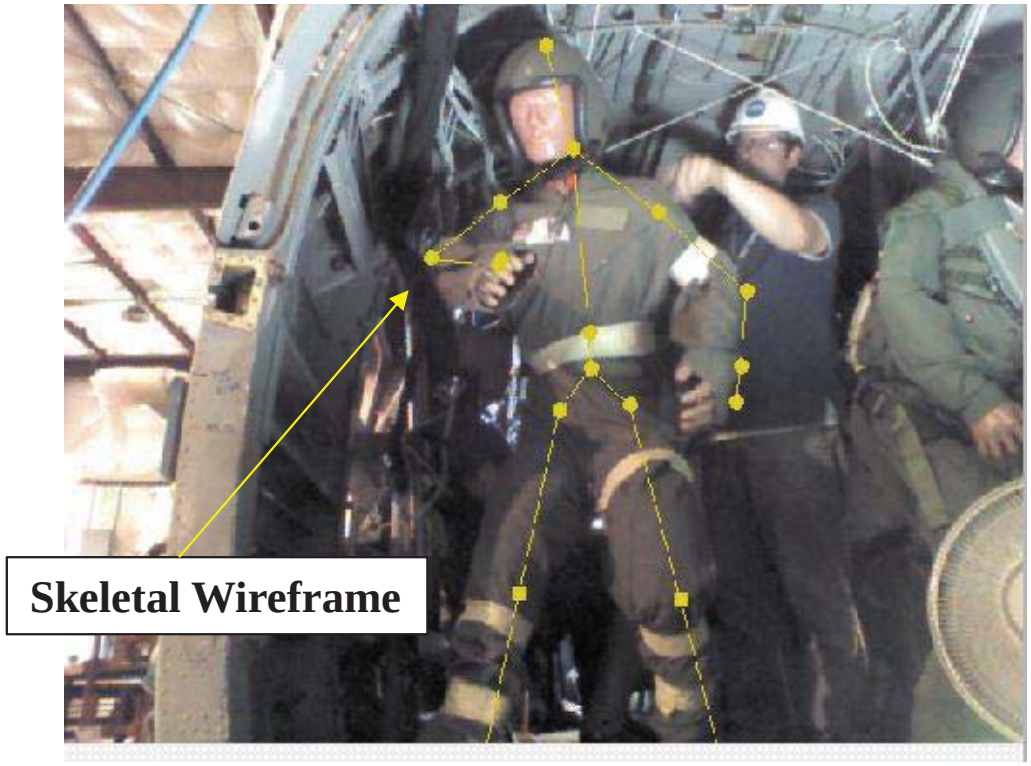

Figure 57. Preliminary ATD wireframe tracking

Test Objective 7 Results for Non-Energy and Energy Absorbing Cargo Restraint

Results for restraint forces in the standard webbing cargo restraint and the load-limiting cargo restraint are shown in Figure 58. The standard webbing cargo restraint developed a tensile load of nearly 5,000 lb. However, there was not enough kinetic energy in the cargo mass for the standard webbing to exceed the breakaway fitting load. The cargo mass was also decelerating in the vertical and longitudinal directions, which differs from typical sled test evaluations. The mass on the standard cargo restraint came to rest without severing the fitting, within 0.060 seconds. The load-limiting cargo restraint exhibited load-limiting behavior about the design load of 3,000 lb. The tensile force plot revealed a loading and unloading behavior as the strap sections ripped and unfolded. The duration of the deceleration was extended to greater than 0.100 seconds.

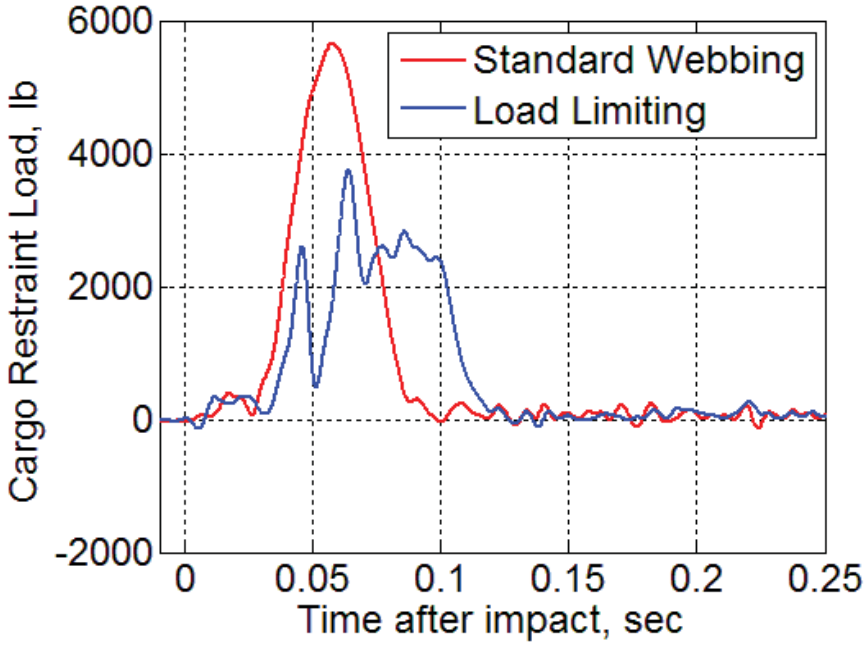

Figure 58. Cargo Restraint Load

Test Objective 8 Results for Three-Tiered Litter

A sequence of images from the high speed camera aimed at the patient litter is shown in Figure 59. During the swing phase, the unloading of the tie-down straps from freefall allowed the upper manikin to shift. The manikin's head was partially suspended off the edge at impact. The manikin and ATD in the middle and lower litter did not move, since the tie-down straps remained in contact with the lower torso. At T+0.060 seconds, there was considerable deformation in the litter covers and longitudinal litter tubes. At T+0.080 seconds, the ceiling mounted strap that supports the aft inboard corner of the upper litter frame detached at the frame, and the litter stack up collapsed. The upper manikin's head impacted the floor and rotated inward and forward with his legs still held with the tie-down straps. The middle ATD fell onto the lower manikin, and flailed freely forward after slackening of the tie-down straps. The lower manikin is impacted by the middle ATD and only shifted slightly forward. Severe injury is likely for all three ATDs.

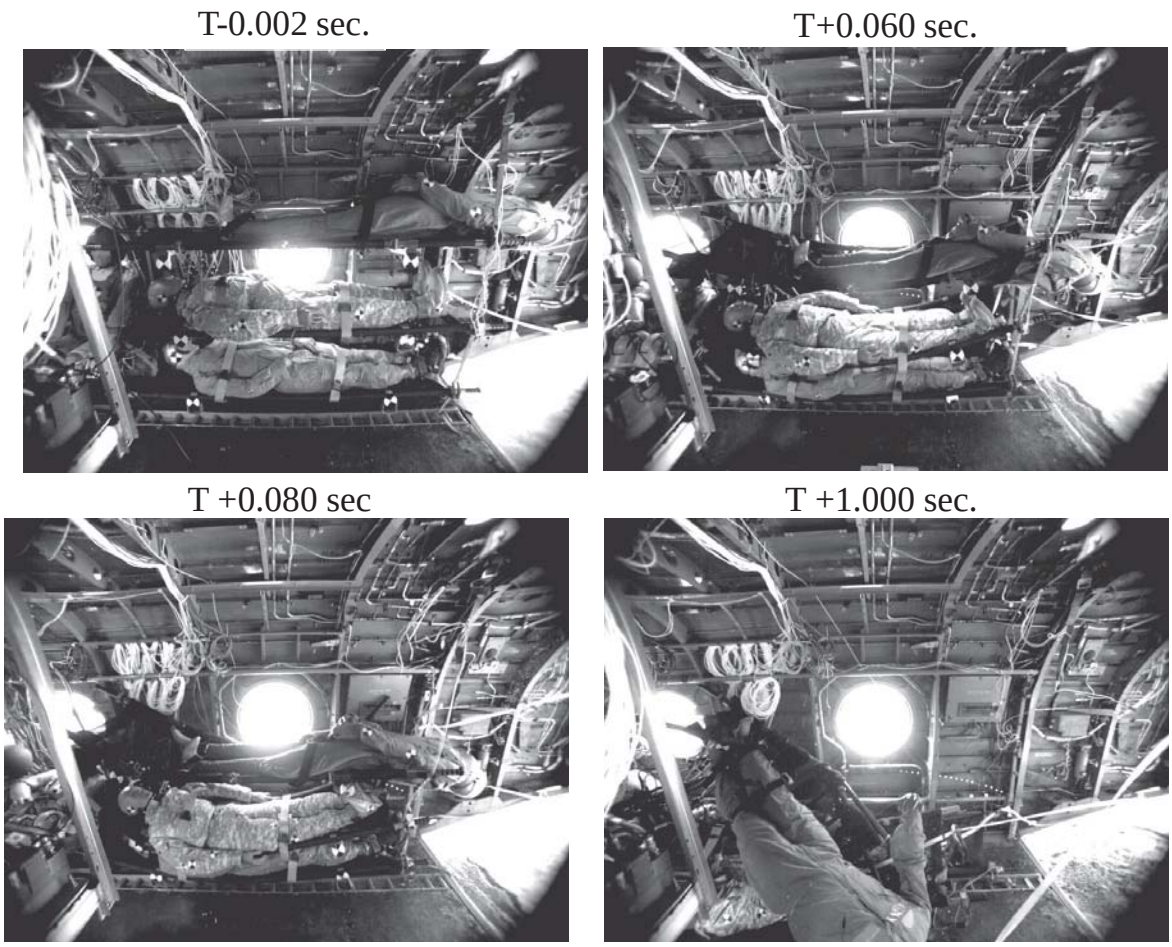

Figure 59. Patient Litter Sequence

CONCLUDING REMARKS

The TRACT 1 test was conducted in August 2013 at the LandIR facility. The impact test conditions (33-ft/s forward and 25-ft/s vertical velocity with a 2.5° nose-up pitch onto soft soil) were considered lower than typical DOD qualification levels, but severe enough to approach civilian requirements. The scenario tested has several parallels in field mishap data, and is believed to be a realistic and plausible condition that represents real world events.

The TRACT 1 test was a highly successful collaboration between the FAA, DOD, and industry. The comprehensive data acquisition and photogrammetry were unprecedented in scope. Over 350 channels of airframe and ATD data were collected with minimal loss of signal. External and onboard high speed and high definition cameras numbering more than 40 cameras provided for coverage not previously feasible in such a test. In addition to airframe structural responses, a total of 8 unique experiments were conducted as part of the crash test. These experiments included:

1. Comparison of ATD responses in a CH-46 crew seat with MA-16 inertia reel versus a CH-46 crew seat with PARS

2. Comparison of floor-mounted passenger seat and ATD responses
3. Comparison of standing ATD with a traditional gunner's belt versus a standing ATD with Aircrew Endurance Vest and MARS
4. Full-field three-dimensional photogrammetry data collection
5. Comparison of sidewall-mounted CACS troop seated Hybrid III ATD, seated Hybrid III ATD with ES-2re head and neck, and two seated Hybrid II ATDs in a standard CH-46 tube and rag sidewall troop seat
6. Evaluation of markerless tracking of ATD response
7. Comparison of cargo experiment with non-energy-absorbing restrained cargo mass and energy absorbing restrained cargo mass
8. Three-tiered litter mounted in the aft starboard region of the aircraft cabin.

The horizontal decelerations were consistent throughout the aircraft at approximately 10-g with a duration of 80 msec. The vertical decelerations within the cabin varied from 20-50 g. The 2.5-degree pitch up attitude caused the cockpit to accelerate downward just prior to belly contact. Vertical seat pan accelerations exceeded 100-g due to the weaker cockpit structure.

ATDs were oriented in forward facing, side facing, and standing positions. The lumbar loads were within acceptable injury limits for the ATDs located in the pilot and co-pilot seats and two side facing CACS seats. The lumbar load for the co-pilot ATD with a PARS active restraint was lower than the lumbar load for the pilot ATD restrained using a standard MA-16 inertia reel. Lumbar loads exceeded injury limits for the four ATDs seated in forward facing passenger seats. While lumbar loads were low for the ATDs seated in the legacy troop bench, severe injury was likely due to tearing of the seat fabric and buckling of the frame. ATDs in the legacy patient litter would have likely sustained severe injury due to failure of the litter stanchions and collapse. Loads for the standing ATD held by the MARS system were within survivable limits, while fatal head blunt trauma occurred for the standing ATD held by the legacy gunner's belt.

The stitched cargo restraint performed well and provided load limiting under longitudinal acceleration. Airframe skin vertical and lateral deformations during impact were computed with high-speed photogrammetry. This technique provides a more comprehensive method than employing strain gages or displacement transducers. Critical locations with high deformation could be readily identified over the entire fuselage skin. The markerless tracking experiment was able to provide position during the swing, but the impact of the ATD on the sensor prevented data acquisition during the impact.

Airframe and experimental data for the TRACT 1 test will be compared to a second test of a CH-46E containing similar experiments and conducted under similar test conditions, except that the airframe will be retrofitted with composite energy absorbing subfloor concepts. The TRACT 2 test will be conducted in late 2014. System-level tests like TRACT have the potential to enhance crashworthy system design, improve current regulations, and enable the next generation of aircraft airframe design.

REFERENCES

1. NASA Rotary Wing Project Overview, Briefing to NASA Langley Research Center, Susan Gorton, November 2012.
2. Anonymous, Military Standard, MIL-STD-1290A (AV), Light Fixed- and Rotary-Wing Aircraft Crash Resistance, Department of Defense, Washington DC, 20301, September 26, 1988.
3. Labun, L., "A Study of Rotary-Wing Crashes to Support New Crashworthiness Criteria," AHS Forum 66, Phoenix, AZ, May 10-13, 2010.
4. Kent, R., "Injury and Fatality Patterns in US Navy Rotary Wing Mishaps: A Descriptive Review of Class A and B Mishaps from 1985 to 2005," AHS Forum 65, Grapevine, TX, May 27-29, 2009.
5. Couch, M. and Lindell, D., "Study on Rotorcraft Safety and Survivability," AHS Forum 66, Phoenix, AZ, May 10-13, 2010.
6. Bolukbasi, A., Crocco J., Clarke, C., Fasanella, E., Jackson, K., Leary, P., Labun, L., Mapes, P., McEntire J., Pellettiere, J., Pilati, B., Rumph, F., Schuck, J., Schultz, M., Smith, M., and Vasquez, D., "Full Spectrum Crashworthiness Criteria for Rotorcraft," RDECOM TR 12-D-12, December 2011.
7. ADS-11B, Aeronautical Design Standard, Survivability Program, Rotary Wing, May 1987.
8. Code of Federal Regulations - Title 14: Aeronautics and Space, Part 29: Airworthiness Standards: Transport Category Rotorcraft, 29.562 - Emergency landing dynamic conditions.
9. Pellettiere, J., and Moorcroft, D., "Aircraft Seat Certification by Analysis from a Regulatory Perspective," Proceedings of the American Helicopter Society 69th Annual Forum, Phoenix, AZ, May 21-23, 2013.
10. DeWeese, R., Moorcroft, D., Abromowitz, A., and Pellettiere, J., "Civil Aircraft Side-Facing Seat Research Summary," DOT/FAA/AM-12/18, November 2012.
11. Code of Federal Regulations - Title 14: Aeronautics and Space, Part 25: Airworthiness Standards: Transport Category Airplanes, 25.562 - Emergency landing dynamic conditions.
12. Podob, R., Happ, M., and Sample, A.,"Mobile Aircrew Restraint System – MARS," Proceedings of the Forty Third Annual SAFE Association Symposium, Salt Lake City, UT, October 24-26, 2005.
13. Thomas, M., Chitty, D., Gildea, M., and T'Kindt, C, "Constitutive Soil Properties for Unwashed Sand and Kennedy Space Center," NASA/CR-2008-215334, July 2008.
14. Society of Automotive Engineers, Recommended Practice: Instrumentation for Impact Test – Part 1, Electronic Instrumentation, SAE J211/1, March 1995.
15. Horta, L. G., Lyle, K. H., Lessard, W. B., "Evaluation of Singular Value Decomposition Approach for Impact Dynamic Data Correlation," NASA TM 2003–212657, October 2003.

16. Richards, M., Podob, R., “Development of an Advanced Energy Absorber,” SAFE Symposium Proceedings, 1997.
17. Eiband, M. A., "Human Tolerance to Rapidly Applied Accelerations: A Summary of the Literature," NASA Memorandum 5–19–59E, June 1959.
18. Brinkley, J. W. and Shaffer, J. T., "Dynamic Simulation Techniques for the Design of Escape Systems: Current Applications and Future Air Force Requirements," Symposium on Biodynamic Models and their Applications, AMRL–TR–71–29, Wright-Patterson Air Force Base, Dayton, OH, Aerospace Medical Research Laboratory, 1970.
19. Eppinger, R., Sun, E., Kuppa, S., and Saul, R., “Supplement: Development of Improved Injury Criteria for the Assessment of Advanced Automotive Restraint Systems – II,” National Highway Traffic Safety Administration, March 2000.

REPORT DOCUMENTATION PAGE

Form Approved
OMB No. 0704-0188

1. REPORT DATE *(DD-MM-YYYY)*	2. REPORT TYPE	3. DATES COVERED *(From - To)*
01- 10 - 2014	Technical Memorandum	

4. TITLE AND SUBTITLE

Evaluation of the First Transport Rotorcraft Airframe Crash Testbed (TRACT 1) Full-Scale Crash Test

5a. CONTRACT NUMBER

5b. GRANT NUMBER

5c. PROGRAM ELEMENT NUMBER

6. AUTHOR(S)

Annett, Martin S.; Littell, Justin D.; Jackson, Karen E.; Bark, Lindley W.; DeWeesse, Rick L.; McEntire, B. Joseph

5d. PROJECT NUMBER

5e. TASK NUMBER

5f. WORK UNIT NUMBER

380046.02.07.04.01.04

7. PERFORMING ORGANIZATION NAME(S) AND ADDRESS(ES)

NASA Langley Research Center
Hampton, VA 23681-2199

8. PERFORMING ORGANIZATION REPORT NUMBER

L-20469

9. SPONSORING/MONITORING AGENCY NAME(S) AND ADDRESS(ES)

National Aeronautics and Space Administration
Washington, DC 20546-0001

10. SPONSOR/MONITOR'S ACRONYM(S)

NASA

11. SPONSOR/MONITOR'S REPORT NUMBER(S)

NASA/TM-2014-218543

12. DISTRIBUTION/AVAILABILITY STATEMENT

Unclassified - Unlimited
Subject Category 39
Availability: NASA CASI (443) 757-5802

13. SUPPLEMENTARY NOTES

14. ABSTRACT

In 2012, the NASA Rotary Wing Crashworthiness Program initiated the Transport Rotorcraft Airframe Crash Testbed (TRACT) research program by obtaining two CH-46E medium lift helicopters from the U.S. Navy. The first crash test (TRACT 1) was performed at NASA Langley Research Center's Landing and Impact Research Facility (LandIR) in August 2013. Crash test conditions represented a severe but potentially survivable impact scenario. A total of 8 unique experiments were conducted to evaluate ATD responses, seat and restraint performance, cargo restraint effectiveness, patient litter behavior, and photogrammetric techniques. A combination of Hybrid II, Hybrid III, and ES-2 Anthropomorphic Test Devices (ATDs) were placed in forward and side facing seats, and in standing positions using mobile aircrew restraints. Occupant results were compared against injury criteria. Loads from ATDs in energy absorbing seats and restraints were within injury limits. Severe injury was likely for ATDs in forward facing passenger seats, legacy troop bench seats, and a three-tiered patient litter. In addition to occupant loading, the structural response of the airframe was assessed based on accelerometers located throughout the airframe and using three-dimensional photogrammetric techniques. Analysis of the photogrammetric data indicated regions of maximum deflection and permanent deformation.

15. SUBJECT TERMS

Energy absorption; Impact testing; Smulation

16. SECURITY CLASSIFICATION OF:			17. LIMITATION OF ABSTRACT	18. NUMBER OF PAGES	19a. NAME OF RESPONSIBLE PERSON
a. REPORT	b. ABSTRACT	c. THIS PAGE			STI Help Desk (email: help@sti.nasa.gov)
					19b. TELEPHONE NUMBER *(Include area code)*
U	U	U	UU	66	(443) 757-5802